Location Sensing and Beamforming Design for IRS-Enabled Multi-User ISAC Systems

Zhouyuan Yu, Xiaoling Hu, *Member, IEEE*, Chenxi Liu, *Senior Member, IEEE*, Mugen Peng, *Fellow, IEEE*, and Caijun Zhong, *Senior Member, IEEE*

***Abstract*—This paper explores the potential of the intelligent reflecting surface (IRS) in realizing multi-user concurrent communication and localization, using the same time-frequency resources. Specifically, we propose an IRS-enabled multi-user integrated sensing and communication (ISAC) framework, where a distributed semi-passive IRS assists the uplink data transmission from multiple users to the base station (BS) and conducts multi-user localization, simultaneously. We first design an ISAC transmission protocol, where the whole transmission period consists of two periods, i.e., the ISAC period for simultaneous uplink communication and multi-user localization, and the pure communication (PC) period for only uplink data transmission. For the ISAC period, we propose a multi-user location sensing algorithm, which utilizes the uplink communication signals unknown to the IRS, thus removing the requirement of dedicated positioning reference signals in conventional location sensing methods. Based on the sensed users' locations, we propose two novel beamforming algorithms for the ISAC period and PC period, respectively, which can work with discrete phase shifts and require no channel state information (CSI) acquisition. Numerical results show that the proposed multi-user location sensing algorithm can achieve up to millimeter-level positioning accuracy, indicating the advantage of the IRS-enabled ISAC framework. Moreover, the proposed beamforming algorithms with sensed location information and discrete phase shifts can achieve comparable performance to the benchmark considering perfect CSI acquisition and continuous phase shifts, demonstrating how the location information can ensure the communication performance.**

***Index Terms*—Integrated sensing and communication (ISAC), intelligent reflecting surface (IRS), multi-user location sensing, discrete phase shifts, joint active and passive beamforming.**

I. Introduction

INTELLIGENT reflecting surface (IRS) is considered as a promising technology for the sixth-generation (6G) mobile communications, owing to its potential of enhancing the capacity and coverage of wireless network by proactively reconfiguring the wireless propagation environment [1]. In general, the IRS is an electromagnetic two-dimensional metasurface composed of a large array of passive reflecting elements, each of which can independently impose the required phase shift on the incident signal to create a desirable multi-path effect [2], [3], [4]. Moreover, the IRS can passively reflect the incident signals without any sophisticated signal processing operations that require radio-frequency (RF) transceiver hardware, thereby significantly reducing hardware cost and energy consumption [5], [6]. Due to the aforementioned attractive characteristics, IRS becomes a focal point of research in wireless communications.

The IRS-aided communications have been extensively investigated under various setups and objectives. By jointly optimizing active and passive beamforming, the IRS can significantly improve the communication performance in terms of spectral efficiency [7], [8], [9], sum rate [10], [11], [12], [13], [14], and energy efficiency [15], [16], [17], [18]. For example, the work [7] considered the spectral efficiency maximization problem via joint active and passive beamforming. Two beamforming algorithms based on fixed point iteration and manifold optimization techniques were respectively proposed for solving this problem. Later on, considering the general multi-user case, the work [10] formulated a weighted sum rate (WSR) maximization problem, which is solved by exploiting the block coordinate descent (BCD) technique. Furthermore, taking the hardware limitation into consideration, the authors in [11] proposed two beamforming algorithms with discrete phase shifts to maximize the sum rate, by invoking the majorization–minimization (MM) method. In addition to improving the spectral efficiency or the sum rate, IRS also has significant advantages in improving energy efficiency. For example, it was shown in [15] that through joint active and passive beamforming, the IRS-assisted MISO communication system can provide up to 300% higher energy efficiency than the relay-assisted one.

In addition to using the IRS for communications, some works explored the potential of the IRS in wireless localization [19], [20], [21], [22], [23], [24], [25]. In [19], the authors first introduced the IRS into wireless localization and derived the Cramer-Rao lower bounds (CRLB) for positioning with IRS. It was proved that the distributed IRS system can achieve better average CRLB than the centralized IRS system. Then, the work [20] investigated an IRS-assisted 2D mmWave positioning system and demonstrated that the positioning accuracy increases

Manuscript received 13 March 2022; revised 30 August 2022; accepted 20 October 2022. Date of publication 3 November 2022; date of current version 9 November 2022. The associate editor coordinating the review of this manuscript and approving it for publication was Dr. Yik-Chung Wu. This work was supported in part by National Key R&D Program of China under Grant 2021YFB2900200, in part by the National Natural Science Foundation of China under Grants 62201084, 62001047, and in part by the Young Elite Scientist Sponsorship Program by China Institute of Communications under Grant 2021QNRC001. *(Corresponding author: Xiaoling Hu.)*

Zhouyuan Yu, Xiaoling Hu, Chenxi Liu, and Mugen Peng are with the State Key Laboratory of Networking and Switching Technology, Beijing University of Posts and Telecommunications, Beijing 100876, China (e-mail: zhouyuanyu@bupt.edu.cn; xiaolinghu@bupt.edu.cn; chenxi.liu@bupt.edu.cn; pmg@bupt.edu.cn).

Caijun Zhong is with the College of Information Science and Electronic Engineering, Zhejiang University, Hangzhou 310027, China (e-mail: caijunzhong@zju.edu.cn).

Digital Object Identifier 10.1109/TSP.2022.3217353

with the number of IRS elements. Later on, a more practical IRS-aided 3D mmWave localization system was studied in [22]. By using the received signal strength (RSS) based positioning technique, an IRS-aided multi-user location sensing algorithm was proposed in [23]. It was shown that with the assistance of the IRS, the localization error is reduced by at least 3 times. Furthermore, through an angle of arrival (AoA) based iterative positioning algorithm, a centimeter-level positioning accuracy was achieved in [24].

All the aforementioned works considered the design of IRS-aided communications and localization, separately. However, it was demonstrated in [26] that there exists a trade-off between communication and localization performance. From this perspective, the work [26] established an IRS-aided joint localization and communication system, where the time allocation ratio for localization is optimized to balance the performance of communication and localization. In this paper, instead of allocating different time slots for communication and localization like [26], we propose to conduct localization and communication at the same time and frequency resources, thereby improving the spectral efficiency of the IRS-aided system, and also propose to use the sensed location information for enhancing communication performance. Specifically, we propose an IRS-enabled multi-user integrated sensing and communication (ISAC) framework, where a distributed semi-passive IRS is deployed to enable multi-user concurrent localization and communication.

The detailed working process of the IRS-enabled multi-user ISAC system is designed, including transmission protocol, multi-user location sensing, and beamforming design. The main contributions of this paper are summarized as follows.

- We construct a novel 3D multi-user ISAC framework based on a distributed IRS architecture to realize simultaneous communication and localization. The whole transmission period is composed of the ISAC period with two time blocks and the pure communication (PC) period. During the ISAC period, the passive sub-IRS assists the uplink transmission between the base station (BS) and multiple users, and meanwhile two semi-passive sub-IRSs conduct multi-user location sensing by using the uplink communication signals sent by multiple users to the BS. The sensed users' locations in the first time block will be used for beamforming design in the second time block. During the PC period, all three sub-IRSs assist the uplink transmission by exploiting the users' locations sensed in the second time block of the ISAC period for beamforming design.
- We propose a multi-user location sensing algorithm based on the uplink communication signals transmitted from multiple users to the BS, thereby removing the requirement of sending dedicated positioning reference signals. Specifically, we first estimate the effective AoA pairs corresponding to user-IRS links. Then, we estimate the path loss corresponding to each pair of effective AoAs. Finally, based on the estimated AoA pairs and their corresponding path losses, an AoA matching algorithm is proposed to determine users' locations.
- We propose two novel beamforming algorithms with discrete phase shifts to maximize the sum rate for the ISAC period and the PC period, respectively, where the sensed location information is exploited for joint active and passive beamforming, thereby avoiding high-overhead channel estimation.
- Simulation results show that the proposed multi-user location sensing algorithm achieves millimeter-level positioning accuracy, demonstrating the benefit of the proposed IRS-enabled ISAC framework in realizing high-accuracy localization. Moreover, the proposed sensing-based beamforming algorithms with sensed users' locations and discrete phase shifts achieve similar performance to the benchmark assuming perfect channel state information (CSI) and continuous phase shifts, validating the effectiveness of beamforming designs using sensed location information.

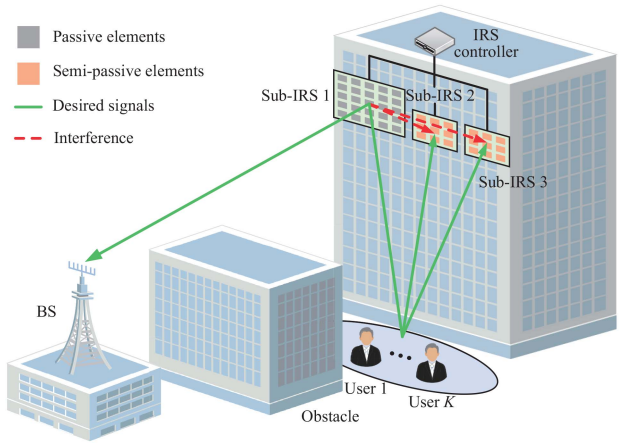

Fig. 1. An IRS-enabled multi-user ISAC system.

The remainder of this paper is organized as follows. Section II introduces the system model of the IRS-aided multi-user ISAC system. Section III presents a multi-user location sensing algorithm, while Section IV presents two sensing-based beamforming algorithms for the ISAC and PC periods, respectively. Section V extends the system to the general multi-IRS case. Numerical results are provided in Section VI. Finally, Section VII concludes this paper.

Notations: Vectors and matrices are denoted by boldface lower case and boldface upper case, respectively. The superscripts $(\cdot)^{\mathrm{T}}$, $(\cdot)^{\mathrm{H}}$, $(\cdot)^{-1}$, $(\cdot)^{\dagger}$, and $(\cdot)^{*}$ denote the operations of transpose, Hermitian transpose, inverse, pseudo-inverse and conjugate, respectively. The Euclidean norm, absolute value, Kronecker product are respectively denoted by $\|\cdot\|$, $|\cdot|$ and $\otimes$. $\mathbb{E}\{\cdot\}$ denotes the statistical expectation. Moreover, $\mathcal{CN}(0,\sigma^2)$ denotes the circularly symmetric complex Gaussian (CSCG) distribution with zero mean and variance σ^2. For matrices, $[\cdot]_{ij}$ denotes the (i,j)-th element of a matrix, $\mathrm{tr}(\cdot)$ represents the matrix trace, $\mathrm{diag}(\cdot)$ denotes a square diagonal matrix with the elements in $(\cdot)$ on its main diagonal, and $\mathbf{1}_{N\times M}$ denotes an $N\times M$ all-one matrix. For vectors, $[\cdot]_i$ denotes the i-th entry of a vector. Besides, j in $e^{j\theta}$ denotes the imaginary unit.

II. System Model

As illustrated in Fig. 1, we consider an IRS-aided multi-user uplink communication system operating in the mmWave band,

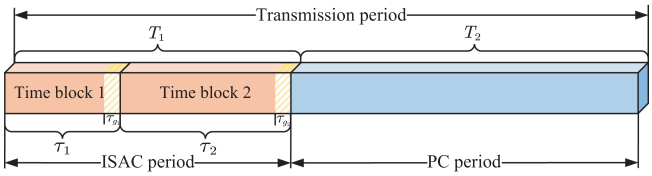

Fig. 2. Illustration of the ISAC transmission protocol.

where a distributed semi-passive IRS with M reflecting elements is deployed to assist the uplink data transmission from K single-antenna users to a multi-antenna BS. We consider that the line-of-sight (LoS) paths between the BS and users are obstructed, and the IRS is deployed to establish strong virtual line-of-sight (VLoS) reflection paths between them. The distributed semi-passive IRS is composed of 3 sub-IRSs. The first sub-IRS is passive and consists of M_1 passive reflecting elements, while the i-th ($i = 2, 3$) sub-IRS is semi-passive and consists of M_i ($M_i \ll M_1$) semi-passive reflecting elements, which are capable of both sensing and reflecting [27], [28], [29], [30]. For ease of practical implementation, the phase shift of IRS takes values from a finite set $\mathcal{F}_b = \{0, \frac{2\pi}{2^b}, \ldots, \frac{2\pi}{2^b}(2^b - 1)\}$, where b is the bit-quantization number. The BS has an N-element uniform linear array (ULA) along the y axis, while the i-th sub-IRS has an $M_{y,i} \times M_{z,i}$ uniform rectangular array (URA) lying on the y-o-z plane. Moreover, there is a backhaul link connecting the BS and the IRS for exchanging information. In this paper, both user-IRS and IRS-BS channels are modeled as quasi-static block-fading channels, which remain almost unchanged during each coherence block but vary from one block to another.

A. ISAC Transmission Protocol

As illustrated in Fig. 2, we consider the transmission period within one coherence block, which is composed of the ISAC period with T_1 time slots and the PC period with T_2 time slots. The ISAC period is divided into time block 1 with τ_1 time slots and time block 2 with τ_2 time slots. During the ISAC period, the passive sub-IRS assists the uplink data transmission by reflecting, and meanwhile the two semi-passive sub-IRSs estimate users' locations based on the communication signals transmitted from multiple users to the BS.[1] Specifically, in the first time block, the passive sub-IRS generates a random phase shift beam due to the unavailability of CSI.[2] In the second time block, the phase shift beam of the passive sub-IRS is properly designed to assist uplink data transmission by utilizing the users' locations obtained in the first time block. During the PC period, all three sub-IRSs operate in the reflecting mode to assist the uplink data transmission. And joint active and passive beamforming is designed, based on more accurate users' locations estimated in the second time block of the ISAC period. In addition, the last τ_{g_i} time slots of the i-th time block are the guard time for location sensing and IRS configuration. Since such time cost is trivial compared to the whole time block, we ignore it hereafter.

B. Channel Model

In general, the IRS operating in the mmWave band is deployed with LoS paths to both the BS and users. Hence, the channel from the i-th sub-IRS to the BS is modeled as [33]

$$\mathbf{H}_{\mathrm{I2B},i} = \alpha_{\mathrm{I2B},i}\mathbf{a}\left(u^{\mathrm{A}}_{\mathrm{I2B},i}\right)\mathbf{b}_i^{\mathrm{H}}\left(u^{\mathrm{D}}_{\mathrm{I2B},i}, v^{\mathrm{D}}_{\mathrm{I2B},i}\right), i = 1, 2, 3, \quad (1)$$

where $\alpha_{\mathrm{I2B},i}$ denotes the complex channel gain for the link from the i-th sub-IRS to the BS, $\mathbf{a}$ and $\mathbf{b}_i$ are the array response vectors for the BS and the i-th sub-IRS, respectively. The two effective angles of departure (AoDs) $u^{\mathrm{D}}_{\mathrm{I2B},i}$ and $v^{\mathrm{D}}_{\mathrm{I2B},i}$ as well as the effective AoA $u^{\mathrm{A}}_{\mathrm{I2B},i}$ are respectively defined as

$$u^{\mathrm{D}}_{\mathrm{I2B},i} = 2\frac{d_{\mathrm{IRS}}}{\lambda}\cos\left(\gamma^{\mathrm{D}}_{\mathrm{I2B},i}\right)\sin\left(\varphi^{\mathrm{D}}_{\mathrm{I2B},i}\right), \quad (2)$$

$$v^{\mathrm{D}}_{\mathrm{I2B},i} = 2\frac{d_{\mathrm{IRS}}}{\lambda}\sin\left(\gamma^{\mathrm{D}}_{\mathrm{I2B},i}\right), \quad (3)$$

$$u^{\mathrm{A}}_{\mathrm{I2B},i} = 2\frac{d_{\mathrm{BS}}}{\lambda}\sin\left(\theta^{\mathrm{A}}_{\mathrm{I2B},i}\right), \quad (4)$$

where λ denotes the carrier wavelength, d_{IRS} and d_{BS} represent the distances between two adjacent reflecting elements of the IRS and two adjacent antennas of the BS, respectively. In addition, $\theta^{\mathrm{A}}_{\mathrm{I2B},i}$ denotes the AoA at the BS, $\gamma^{\mathrm{D}}_{\mathrm{I2B},i}$ and $\varphi^{\mathrm{D}}_{\mathrm{I2B},i}$ are the elevation and azimuth AoDs for the link from the i-th sub-IRS to the BS, respectively.

Similarly, the channel from the k-th user to the i-th sub-IRS is modeled as

$$\mathbf{h}_{\mathrm{U2I},i,k} = \alpha_{\mathrm{U2I},i,k}\mathbf{b}_i\left(u^{\mathrm{A}}_{\mathrm{U2I},i,k}, v^{\mathrm{A}}_{\mathrm{U2I},i,k}\right), \quad i = 1, 2, 3,\ k = 1, \ldots, K, \quad (5)$$

where $\alpha_{\mathrm{U2I},i,k}$ denotes the complex channel gain for the link from the k-th user to the i-th sub-IRS, and the two effective AoAs from the k-th user to the i-th sub-IRS are defined as

$$u^{\mathrm{A}}_{\mathrm{U2I},i,k} = 2\frac{d_{\mathrm{IRS}}}{\lambda}\cos\left(\gamma^{\mathrm{A}}_{\mathrm{U2I},i,k}\right)\sin\left(\varphi^{\mathrm{A}}_{\mathrm{U2I},i,k}\right), \quad (6)$$

$$v^{\mathrm{A}}_{\mathrm{U2I},i,k} = 2\frac{d_{\mathrm{IRS}}}{\lambda}\sin\left(\gamma^{\mathrm{A}}_{\mathrm{U2I},i,k}\right), \quad (7)$$

where $\gamma^{\mathrm{A}}_{\mathrm{U2I},i,k}/\varphi^{\mathrm{A}}_{\mathrm{U2I},i,k}$ denotes the elevation/azimuth AoAs for the link from the k-th user to the i-th sub-IRS.

Also, the channel from the passive sub-IRS to the i-th sub-IRS is modeled as

$$\mathbf{H}_{\mathrm{I2I},i} = \alpha_{\mathrm{I2I},i}\mathbf{b}_i\left(u^{\mathrm{A}}_{\mathrm{I2I},i}, v^{\mathrm{A}}_{\mathrm{I2I},i}\right)\mathbf{b}_1^{\mathrm{H}}\left(u^{\mathrm{D}}_{\mathrm{I2I},i}, v^{\mathrm{D}}_{\mathrm{I2I},i}\right), i = 2, 3, \quad (8)$$

where $\alpha_{\mathrm{I2I},i}$ denotes the complex channel gain for the link from the passive sub-IRS to the i-th sub-IRS. In addition, the two effective AoAs $u^{\mathrm{A}}_{\mathrm{I2I},i}$ and $v^{\mathrm{A}}_{\mathrm{I2I},i}$ as well as the two effective AoDs $u^{\mathrm{D}}_{\mathrm{I2I},i}$ and $v^{\mathrm{D}}_{\mathrm{I2I},i}$ are respectively defined as

$$u^{\mathrm{A}}_{\mathrm{I2I},i} = 2\frac{d_{\mathrm{IRS}}}{\lambda}\cos\left(\gamma^{\mathrm{A}}_{\mathrm{I2I},i}\right)\sin\left(\varphi^{\mathrm{A}}_{\mathrm{I2I},i}\right), \quad (9)$$

[1] Although there are some works [31], [32] that considered LoS scenarios and conducted the sensing task at the BS, they can not be applied directly in the considered blind-zone case, where the direct link from the user to the BS is blocked. Hence, we introduce the semi-passive sub-IRSs as anchors (positioning reference points), at which the localization task are performed.

[2] During the i-th ($i > 1$) transmission period, the users' locations estimated in the $(i-1)$-th transmission period would be used to design the phase shift of the passive sub-IRS in the first time block of the ISAC period.

$$v_{\mathrm{I2I},i}^{\mathrm{A}} = 2\frac{d_{\mathrm{IRS}}}{\lambda}\sin\left(\gamma_{\mathrm{I2I},i}^{\mathrm{A}}\right), \tag{10}$$

$$u_{\mathrm{I2I},i}^{\mathrm{D}} = 2\frac{d_{\mathrm{IRS}}}{\lambda}\cos\left(\gamma_{\mathrm{I2I},i}^{\mathrm{D}}\right)\sin\left(\varphi_{\mathrm{I2I},i}^{\mathrm{D}}\right), \tag{11}$$

$$v_{\mathrm{I2I},i}^{\mathrm{D}} = 2\frac{d_{\mathrm{IRS}}}{\lambda}\sin\left(\gamma_{\mathrm{I2I},i}^{\mathrm{D}}\right), \tag{12}$$

where $\gamma_{\mathrm{I2I},i}^{\mathrm{A}}$/ $\varphi_{\mathrm{I2I},i}^{\mathrm{A}}$ denotes the elevation/azimuth AoA and $\gamma_{\mathrm{I2I},i}^{\mathrm{D}}$/$\varphi_{\mathrm{I2I},i}^{\mathrm{D}}$ denotes the elevation/azimuth AoD from the passive sub-IRS to the i-th sub-IRS.

Furthermore, we consider that $d_{\mathrm{BS}} = d_{\mathrm{IRS}} = \frac{\lambda}{2}$. As such, the array response vectors for the BS and the i-th sub-IRS are respectively given by

$$\mathbf{a}(u) = \left[1, \ldots, e^{j\pi(n-1)u}, \ldots, e^{j\pi(N-1)u}\right]^{\mathrm{T}}, \tag{13}$$

$$\mathbf{b}_i(u,v) = \left[1, \ldots, e^{j\pi(n-1)u}, \ldots, e^{j\pi(M_{y,i}-1)u}\right]^{\mathrm{T}} \otimes \left[1, \ldots, e^{j\pi(m-1)v}, \ldots, e^{j\pi(M_{z,i}-1)v}\right]^{\mathrm{T}}. \tag{14}$$

C. Signal Model

1) ISAC Period: In the ISAC period, only the passive sub-IRS (i.e., the first sub-IRS) operates in the reflecting mode to assist uplink transmission. During the n-th time block, the k-th user sends $\sqrt{\rho}s_k(t)$, satisfying $|s_k(t)| = 1$, to the BS at time slot $t \in \mathcal{N}_n = \{(n-1)\tau_1 + 1, \ldots, \tau_1 + (n-1)\tau_2\}$, where ρ denotes the transmit power. The received signal at the BS is given by

$$y(t) = \sqrt{\rho}\sum_{k=1}^{K}\left[\mathbf{w}_k^{(n)}\right]^{\mathrm{H}}\mathbf{H}_{\mathrm{I2B},1}\mathbf{\Theta}_1^{(n)}\mathbf{h}_{\mathrm{U2I},1,k}\ s_k(t) + \sum_{k=1}^{K}\left[\mathbf{w}_k^{(n)}\right]^{\mathrm{H}}\mathbf{n}_{\mathrm{BS}}(t),\ t \in \mathcal{N}_n,\ n = 1,2, \tag{15}$$

where $\mathbf{w}_k^{(n)}$, satisfying $\|\mathbf{w}_k^{(n)}\| = 1$, represents the BS combining vector of the k-th user in the n-th time block. The phase shift matrix of the first sub-IRS in the n-th time block is defined as $\mathbf{\Theta}_1^{(n)} = \mathrm{diag}(\boldsymbol{\xi}_1^{(n)})$, with the phase shift beam being $\boldsymbol{\xi}_1^{(n)} = [e^{j\vartheta_{1,1}^{(n)}}, \ldots, e^{j\vartheta_{1,m}^{(n)}}, \ldots, e^{j\vartheta_{1,M_1}^{(n)}}]^{\mathrm{T}}$. In addition, $\mathbf{n}_{\mathrm{BS}}$ represents the additive white Gaussian noise (AWGN) at the BS, whose elements follow the complex Gaussian distribution $\mathcal{CN}(0, \sigma_0^2)$.

The two semi-passive sub-IRSs operate in the sensing mode, and the received signal at the i-th sub-IRS is given by

$$\mathbf{x}_i(t) = \sqrt{\rho}\sum_{k=1}^{K}\mathbf{h}_{\mathrm{U2I},i,k}\ s_k(t) + \sqrt{\rho}\mathbf{H}_{\mathrm{I2I},i}\mathbf{\Theta}_1^{(n)}\sum_{k=1}^{K}\mathbf{h}_{\mathrm{U2I},1,k}\ s_k(t) + \mathbf{n}_i(t),\ i = 2,3,\ t \in \mathcal{N}_n,\ n = 1,2, \tag{16}$$

where $\mathbf{n}_i$ represents the AWGN at the i-th sub-IRS, whose elements follow the complex Gaussian distribution $\mathcal{CN}(0, \sigma_0^2)$.

The instantaneous achievable rate of the k-th user during the ISAC period is given by

$$R_k(t) = \log_2\left(1 + \frac{\rho\left|\left[\mathbf{w}_k^{(n)}\right]^{\mathrm{H}}\mathbf{H}_{\mathrm{I2B},1}\mathbf{\Theta}_1^{(n)}\mathbf{h}_{\mathrm{U2I},1,k}\right|^2}{\rho\sum_{j\neq k}^{K}\left|\left[\mathbf{w}_k^{(n)}\right]^{\mathrm{H}}\mathbf{H}_{\mathrm{I2B},1}\mathbf{\Theta}_1^{(n)}\mathbf{h}_{\mathrm{U2I},1,j}\right|^2 + \sigma_0^2}\right),\ t \in \mathcal{N}_n,\ n = 1,2. \tag{17}$$

2) PC Period: In the PC period, all three sub-IRSs operate in the reflecting mode to assist uplink transmission. The k-th user sends $\sqrt{\rho}s_k(t)$ to the BS at time slot $t \in \mathcal{T}_2 \triangleq \{T_1 + 1, \ldots, T_1 + T_2\}$. The received signal at the BS is

$$y(t) = \sqrt{\rho}\sum_{k=1}^{K}\mathbf{w}_k^{\mathrm{H}}(t)\mathbf{H}_{\mathrm{I2B}}\mathbf{\Theta}(t)\mathbf{h}_{\mathrm{U2I},k}\ s_k(t) + \sum_{k=1}^{K}\mathbf{w}_k^{\mathrm{H}}(t)\mathbf{n}_{\mathrm{BS}}(t),\ t \in \mathcal{T}_2, \tag{18}$$

where $\mathbf{H}_{\mathrm{I2B}} \triangleq [\mathbf{H}_{\mathrm{I2B},1}, \mathbf{H}_{\mathrm{I2B},2}, \mathbf{H}_{\mathrm{I2B},3}] \in \mathbb{C}^{N\times M}$ and $\mathbf{h}_{\mathrm{U2I},k} \triangleq [\mathbf{h}_{\mathrm{U2I},1,k}^{\mathrm{T}}, \mathbf{h}_{\mathrm{U2I},2,k}^{\mathrm{T}}, \mathbf{h}_{\mathrm{U2I},3,k}^{\mathrm{T}}]^{\mathrm{T}} \in \mathbb{C}^{M\times 1}$ denote the baseband equivalent channels from the IRS to the BS and from the k-th user to the IRS, respectively. The phase shift matrix of the whole IRS is defined as $\mathbf{\Theta}(t) = \mathrm{diag}(\boldsymbol{\xi}(t))$, where $\boldsymbol{\xi}(t) \triangleq [\boldsymbol{\xi}_1^{\mathrm{T}}(t), \boldsymbol{\xi}_2^{\mathrm{T}}(t), \boldsymbol{\xi}_3^{\mathrm{T}}(t)]^{\mathrm{T}}$ with the phase shift beam being $\boldsymbol{\xi}_i(t) = [e^{j\vartheta_{i,1}(t)}, \ldots, e^{j\vartheta_{i,m}(t)}, \ldots, e^{j\vartheta_{i,M_i}(t)}]^{\mathrm{T}}$.

The instantaneous achievable rate of the k-th user during the PC period is given by

$$R_k(t) = \log_2\left(1 + \frac{\rho\left|\mathbf{w}_k^{\mathrm{H}}(t)\mathbf{H}_{\mathrm{I2B}}\mathbf{\Theta}(t)\mathbf{h}_{\mathrm{U2I},k}\right|^2}{\rho\sum_{j\neq k}^{K}\left|\mathbf{w}_k^{\mathrm{H}}(t)\mathbf{H}_{\mathrm{I2B}}\mathbf{\Theta}(t)\mathbf{h}_{\mathrm{U2I},j}\right|^2 + \sigma_0^2}\right),\ t \in \mathcal{T}_2. \tag{19}$$

III. Multi-User Location Sensing

In this section, we design a multi-user location sensing algorithm based on the received communication signals at the two semi-passive sub-IRSs. Specifically, we first estimate the effective AoA pairs at the two semi-passive IRSs, by combining the use of the forward-backward spatial smoothing (FBSS) technique, the total least squares-estimation of signal parameters via rotational invariance technique (TLS-ESPRIT), and the multiple signal classification (MUSIC) technique [34]. After excluding the AoA pairs corresponding to the links from the passive sub-IRS to the two semi-passive sub-IRSs, we obtain the effective AoA pairs corresponding to the links from multiple users to the semi-passive sub-IRSs. Then, we estimate the path losses corresponding to these effective AoA pairs. Finally, based on the estimated effective AoA pairs and their corresponding path losses, an AoA matching algorithm is proposed to determine users' locations.

A. Estimate Effective AoAs

To reduce the coherency of the received signals at the semi-passive sub-IRS, we first adopt the FBSS technique to preprocess

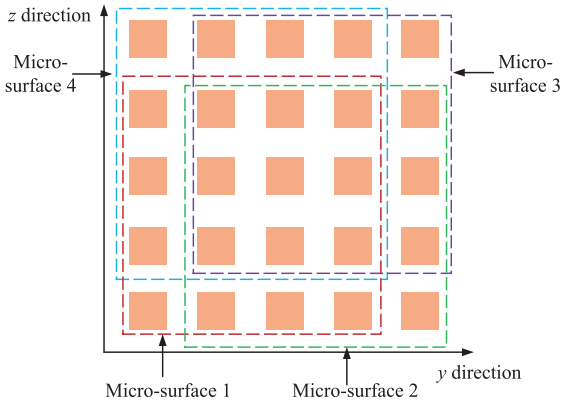

Fig. 3. An example of the micro-surface.

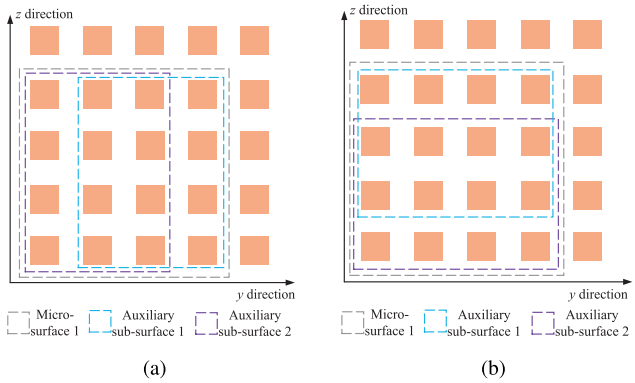

Fig. 4. An example of the auxiliary sub-surface.

the received signals. Then, we separately estimate the effective AoAs corresponding to the y axis (i.e., $u^{\mathrm{A}}_{\mathrm{U2I},i,k}$ and $u^{\mathrm{A}}_{\mathrm{I2I},i}$) and the z axis (i.e., $v^{\mathrm{A}}_{\mathrm{U2I},i,k}$ and $v^{\mathrm{A}}_{\mathrm{I2I},i}$), by invoking the TLS-ESPRIT algorithm. Finally, we pair the effective AoAs corresponding to the y axis with those corresponding to the z axis by invoking the MUSIC algorithm.

1) Preprocess the Received Signals by Using the FBSS Technique: Without loss of generality, we focus on the estimation of the effective AoAs at the i-th sub-IRS in the n-th time block ($i \in \{2,3\}$ and $n \in \{1,2\}$). We construct a set of $N_{\mathrm{micro},i}$ micro-surfaces for the i-th sub-IRS. Each micro-surface is composed of $L_{\mathrm{micro},i} = Q_{y,i} \times Q_{z,i}$ semi-passive elements and shifted by one row along the z direction or one column along the y direction from the preceding micro-surface. For example, we construct a set of 4 micro-surfaces each with 4×4 semi-passive elements, as illustrated in Fig. 3.

Denote the received signals at the m-th micro-surface of the i-th sub-IRS during the n-th time block by $\mathbf{x}_{i,m}(t) \in \mathbb{C}^{L_{\mathrm{micro},i}\times 1}, t \in \mathcal{N}_n$, and define their auto-correlation matrix as $\mathbf{R}^{(n)}_{\mathrm{micro},i} \triangleq \mathbb{E}\{\mathbf{x}_{i,m}(t)[\mathbf{x}_{i,m}(t)]^{\mathrm{H}}\}, t \in \mathcal{N}_n$. According to the FBSS technique, we estimate $\mathbf{R}^{(n)}_{\mathrm{micro},i}$ as

$$\hat{\mathbf{R}}^{(n)}_{\mathrm{micro},i} = \frac{1}{2\tau_n N_{\mathrm{micro},i}} \sum_{t\in\mathcal{N}_n}\sum_{m=1}^{N_{\mathrm{micro},i}} \Big\{ \mathbf{x}_{i,m}(t)\left[\mathbf{x}_{i,m}(t)\right]^{\mathrm{H}} + \mathbf{J}\left[\mathbf{x}_{i,m}(t)\right]^{*}\left[\mathbf{x}_{i,m}(t)\right]^{\mathrm{T}}\mathbf{J} \Big\}, \quad (20)$$

where $\mathbf{J}$ denotes the exchange matrix, with the 1 elements residing on its counterdiagonal and all other elements being zero. Then, we perform eigenvalue decomposition of $\hat{\mathbf{R}}^{(n)}_{\mathrm{micro},i}$

$$\hat{\mathbf{R}}^{(n)}_{\mathrm{micro},i} = \mathbf{U}^{(n)}_i \mathrm{diag}\left(\lambda^{(n)}_{i,1},\ldots,\lambda^{(n)}_{i,L_{\mathrm{micro},i}}\right)\left[\mathbf{U}^{(n)}_i\right]^{\mathrm{H}}, \quad (21)$$

where $\mathbf{U}^{(n)}_i \triangleq \left[\mathbf{u}^{(n)}_{i,1},\ldots,\mathbf{u}^{(n)}_{i,L_{\mathrm{micro},i}}\right]$ and the eigenvalues $\lambda^{(n)}_{i,1}, \ldots, \lambda^{(n)}_{i,L_{\mathrm{micro},i}}$ are in descending order.

2) Estimate $u^{\mathrm{A}}_{\mathrm{U2I},i,k}$ and $u^{\mathrm{A}}_{\mathrm{I2I},i}$ by Using the TLS ESPRIT Algorithm: As shown in Fig. 4(a), for the first micro-surface of the i-th sub-IRS, we construct two auxiliary sub-surfaces each with $L_{\mathrm{aux},i} = (Q_{y,i}-1)\times Q_{z,i}$ semi-passive elements, satisfying $L_{\mathrm{aux},i} \geqslant K+2$. The signal sub-space corresponding to the two auxiliary sub-surfaces is given by

$$\mathbf{U}^{(n)}_{\mathrm{S},im} \triangleq \mathbf{J}_m \mathbf{U}^{(n)}_{\mathrm{S},i}, m = 1,2, \quad (22)$$

where $\mathbf{U}^{(n)}_{\mathrm{S},i} \triangleq \left[\mathbf{u}^{(n)}_{i,1},\ldots,\mathbf{u}^{(n)}_{i,K+1}\right] \in \mathbb{C}^{L_{\mathrm{micro},i}\times(K+1)}$, $\mathbf{J}_m \in \mathbb{R}^{L_{\mathrm{aux},i}\times L_{\mathrm{micro},i}}$ is a selecting matrix whose elements are either 1 or 0. If the j-th reflecting element of the micro-surface 1 is selected as the i-th element of the auxiliary sub-surface m, then we set $[\mathbf{J}_m]_{ij} = 1$. Otherwise, we set $[\mathbf{J}_m]_{ij} = 0$.

Then, we define $\mathbf{C}^{(n)}_i \triangleq \left[\mathbf{U}^{(n)}_{\mathrm{S},i1}, \mathbf{U}^{(n)}_{\mathrm{S},i2}\right]^{\mathrm{H}}\left[\mathbf{U}^{(n)}_{\mathrm{S},i1}, \mathbf{U}^{(n)}_{\mathrm{S},i2}\right] \in \mathbb{C}^{(2K+2)\times(2K+2)}$ and perform eigendecomposition of it, which yields

$$\mathbf{C}^{(n)}_i = \begin{bmatrix}\mathbf{V}^{(n)}_{i,11} & \mathbf{V}^{(n)}_{i,12}\\ \mathbf{V}^{(n)}_{i,21} & \mathbf{V}^{(n)}_{i,22}\end{bmatrix}\mathbf{\Lambda}^{(n)}_{C,i}\begin{bmatrix}\mathbf{V}^{(n)}_{i,11} & \mathbf{V}^{(n)}_{i,12}\\ \mathbf{V}^{(n)}_{i,21} & \mathbf{V}^{(n)}_{i,22}\end{bmatrix}^{\mathrm{H}}, \quad (23)$$

where $\mathbf{\Lambda}^{(n)}_{C,i} \triangleq \mathrm{diag}\left(\lambda^{(n)}_{\mathrm{C},i1},\ldots,\lambda^{(n)}_{\mathrm{C},i(2K+2)}\right)$ with its eigenvalues in descending order, $\mathbf{V}^{(n)}_{i,12}$ and $\mathbf{V}^{(n)}_{i,22}$ are two $(K+1)\times(K+1)$ matrices.

After obtaining $\mathbf{V}^{(n)}_{i,12}$ and $\mathbf{V}^{(n)}_{i,22}$, we calculate

$$\mathbf{\Phi}^{(n)}_{\mathrm{TLS},i} = -\mathbf{V}^{(n)}_{i,12}\left[\mathbf{V}^{(n)}_{i,22}\right]^{-1}. \quad (24)$$

By performing eigenvalue decomposition of $\mathbf{\Phi}^{(n)}_{\mathrm{TLS},i}$, we obtain its eigenvalues as $\lambda^{(n)}_{\mathrm{TLS},il}, l = 1,\ldots,K+1$.

Finally, we estimate the effective AoAs at the i-th sub-IRS corresponding to the y axis as

$$\breve{u}^{(n)}_{il} = \mathrm{angle}\left(\lambda^{(n)}_{\mathrm{TLS},il}\right), l = 1,\ldots,K+1. \quad (25)$$

The estimators of $u^{\mathrm{A}}_{\mathrm{U2I},i,k}$ and $u^{\mathrm{A}}_{\mathrm{I2I},i}$ in the n-th time block belong to $\mathcal{U}^{(n)}_i \triangleq \{\breve{u}^{(n)}_{il}, l=1,\ldots,K+1\}$, i.e., $\hat{u}^{\mathrm{A},(n)}_{\mathrm{U2I},i,k}, \hat{u}^{\mathrm{A},(n)}_{\mathrm{I2I},i} \in \mathcal{U}^{(n)}_i$.

3) Estimate $v^{\mathrm{A}}_{\mathrm{U2I},i,k}$ and $v^{\mathrm{A}}_{\mathrm{I2I},i}$ by Using the TLS-ESPRIT Algorithm: As shown in Fig. 4(b), for the first micro-surface of the i-th sub-IRS, we construct two auxiliary sub-surfaces each with $\tilde{L}_{\mathrm{aux},i} = Q_{y,i}\times(Q_{z,i}-1)$ semi-passive elements, satisfying $\tilde{L}_{\mathrm{aux},i} \geqslant K+2$. Following the similar process of estimating $u^{\mathrm{A}}_{\mathrm{U2I},i,k}$ and $u^{\mathrm{A}}_{\mathrm{I2I},i}$, we estimate the effective AoAs at the i-th sub-IRS corresponding to the z axis as $\breve{v}^{(n)}_{il}, l = 1,\ldots,K+1$. The

estimators of $v_{\mathrm{U2I},i,k}^{\mathrm{A}}$ and $v_{\mathrm{I2I},i}^{\mathrm{A}}$ in the n-th time block belong to $\mathcal{V}_i^{(n)} \triangleq \{\check{v}_{il}^{(n)}, l=1,\ldots,K+1\}$, i.e., $\hat{v}_{\mathrm{U2I},i,k}^{\mathrm{A},(n)}, \hat{v}_{\mathrm{I2I},i}^{\mathrm{A},(n)} \in \mathcal{V}_i^{(n)}$.

4) Pair $\check{u}_{il}^{(n)}$ and $\check{v}_{il}^{(n)}$ by Using the MUSIC Algorithm: Let

$$\check{f}_{i,ls}^{(n)} \triangleq \mathbf{b}_{\mathrm{micro},i}^{\mathrm{H}}\left(\check{u}_{il}^{(n)}, \check{v}_{is}^{(n)}\right)\mathbf{U}_{\mathrm{N},i}^{(n)}, \tag{26}$$

where $\mathbf{U}_{\mathrm{N},i}^{(n)} \triangleq \left[\mathbf{u}_{i,(K+2)}^{(n)},\ldots,\mathbf{u}_{i,L_{\mathrm{micro},i}}^{(n)}\right]$, and $\mathbf{b}_{\mathrm{micro},i}$ denotes the array response vector of the micro-surface on the i-th sub-IRS. Then, we compute

$$f\left(\check{u}_{il}^{(n)}, \check{v}_{is}^{(n)}\right) = \check{f}_{i,ls}^{(n)}\left[\check{f}_{i,ls}^{(n)}\right]^{\mathrm{H}}, l,s=1,\ldots,K+1, \tag{27}$$

and choose the $K+1$ minima $f(\hat{u}_{il}^{(n)}, \hat{v}_{il}^{(n)})$, $l=1,\ldots,K+1$, where $\hat{u}_{il}^{(n)} \in \mathcal{U}_i^{(n)}$ and $\hat{v}_{il}^{(n)} \in \mathcal{V}_i^{(n)}$. As such, we obtain $K+1$ pairs of effective AoAs $(\hat{u}_{il}^{(n)}, \hat{v}_{il}^{(n)}), l=1,\ldots,K+1$.

5) Determine the AoA Pairs Corresponding to the Links From Users to Semi-Passive sub-IRSs: Denote the locations of the BS and the i-th sub-IRS by $\mathbf{q}_{\mathrm{BS}} = (x_{\mathrm{BS}}, y_{\mathrm{BS}}, z_{\mathrm{BS}})$ and $\mathbf{q}_i = (x_i, y_i, z_i)$, respectively. Due to the fixed locations of the BS and the sub-IRS, we assume that their locations are perfectly known. Therefore, the effective AoAs from the passive sub-IRS to the i-th ($i=2, 3$) sub-IRS can be calculated as

$$u_{\mathrm{I2I},i}^{\mathrm{A}} = \frac{y_i - y_1}{\|\mathbf{q}_i - \mathbf{q}_1\|},\ v_{\mathrm{I2I},i}^{\mathrm{A}} = \frac{z_i - z_1}{\|\mathbf{q}_i - \mathbf{q}_1\|}. \tag{28}$$

After excluding the AoA pair corresponding to $(u_{\mathrm{I2I},i}^{\mathrm{A}}, v_{\mathrm{I2I},i}^{\mathrm{A}})$ from $\{(\hat{u}_{il}^{(n)}, \hat{v}_{il}^{(n)}), l=1,\ldots,K+1\}$, the i-th sub-IRS obtains K pairs of effective AoAs corresponding to K users, the set of which is denoted by $\mathcal{A}_i \triangleq \{(\hat{u}_{il}^{(n)}, \hat{v}_{il}^{(n)}) | \, l=1,\ldots,K\}, i=2,3$.

B. Determine Users' Locations

For the effective AoA pair $\left(\hat{u}_{2\,l}^{(n)}, \hat{v}_{2\,l}^{(n)}\right)$ in $\mathcal{A}_2$, we should find the effective AoA pair in $\mathcal{A}_3$, so that the two effective AoA pairs are corresponding to the same user. As such, the user location can be determined by these two AoA pairs. In the following, we first estimate the path losses corresponding to the $2K$ AoA pairs that belong to $\mathcal{A}_2$ or $\mathcal{A}_3$. Then, K^2 possible users' locations and their corresponding path losses are computed. Based on the estimated $2K$ path losses and the calculated K^2 possible path losses, an AoA matching algorithm is proposed to determine users' locations.

1) Estimate the Path Loss Corresponding to Each Pair of Effective AoAs: According to (5) and (8), the received signal at the i-th sub-IRS during the n-th time block of the ISAC period can be rewritten as (29) shown at the bottom of this page, where the first term denotes the interference from the passive sub-IRS, the second term denotes the signals from K users to the i-th sub-IRS, and the third term is the AWGN at the i-th sub-IRS.

Define $P_i \triangleq \alpha_{\mathrm{I2I},i}\mathbf{b}_1^{\mathrm{H}}(u_{\mathrm{I2I},i}^{\mathrm{D}}, v_{\mathrm{I2I},i}^{\mathrm{D}})\mathbf{\Theta}_1^{(n)}\sum_{k=1}^{K}\alpha_{\mathrm{U2I},1,k}s_k(t)\,\mathbf{b}_1(u_{\mathrm{U2I},1,k}^{\mathrm{A}}, v_{\mathrm{U2I},1,k}^{\mathrm{A}})$, and (29) can be compactly written as

$$\mathbf{x}_i^{(n)}(t) = \sqrt{\rho}\mathbf{B}_i\boldsymbol{\beta}_i\mathbf{s} + \mathbf{n}_i(t),\ i=2,3,\ t\in\mathcal{N}_n,\ n=1,2, \tag{30}$$

where

$$\mathbf{B}_i \triangleq \left[\mathbf{b}_i\left(u_{\mathrm{U2I},i,1}^{\mathrm{A}}, v_{\mathrm{U2I},i,1}^{\mathrm{A}}\right),\ldots,\mathbf{b}_i\left(u_{\mathrm{U2I},i,K}^{\mathrm{A}}, v_{\mathrm{U2I},i,K}^{\mathrm{A}}\right),\ \mathbf{b}_i\left(u_{\mathrm{I2I},i}^{\mathrm{A}}, v_{\mathrm{I2I},i}^{\mathrm{A}}\right)\right] \in \mathbb{C}^{M_i\times(K+1)}, \tag{31}$$

$$\boldsymbol{\beta}_i \triangleq \mathrm{diag}\left(\alpha_{\mathrm{U2I},i,1},\ldots,\alpha_{\mathrm{U2I},i,K},P_i\right) \in \mathbb{C}^{(K+1)\times(K+1)}, \tag{32}$$

$$\mathbf{s} \triangleq [s_1(t),\ldots,s_K(t),1]^{\mathrm{T}} \in \mathbb{C}^{(K+1)\times 1}. \tag{33}$$

Since $|s_k(t)|=1$ and $\mathbb{E}\{s_i(t)s_j(t)\}=0, i\neq j$, the auto-correlation matrix of $\mathbf{x}_i^{(n)}(t)$ can be expressed as

$$\mathbf{R}_i^{(n)} \triangleq \mathbb{E}\left\{\mathbf{x}_i^{(n)}(t)\left[\mathbf{x}_i^{(n)}(t)\right]^{\mathrm{H}}\right\} = \rho\mathbf{B}_i\mathbf{R}_{\boldsymbol{\beta}_i}\mathbf{B}_i^{\mathrm{H}} + \sigma_0^2\mathbf{I}, \tag{34}$$

where $\mathbf{R}_{\boldsymbol{\beta}_i} \triangleq \boldsymbol{\beta}_i\boldsymbol{\beta}_i^{\mathrm{H}} = \mathrm{diag}(|\alpha_{\mathrm{U2I},i,1}|^2,\ldots,|\alpha_{\mathrm{U2I},i,K}|^2,|P_i|^2)$.

Noticing that the path losses are determined by the diagonal elements of $\mathbf{R}_{\boldsymbol{\beta}_i}$, we use (34) and estimate $\mathbf{R}_{\boldsymbol{\beta}_i}$ in the n-th time block as (35) shown at the bottom of next page, where

$$\hat{\mathbf{R}}_i^{(n)} = \frac{1}{\tau_n}\sum_{t\in\mathcal{N}_n}\mathbf{x}_i^{(n)}(t) * \left[\mathbf{x}_i^{(n)}(t)\right]^{\mathrm{H}}, \tag{36}$$

$$\hat{\mathbf{B}}_i^{(n)} = \left[\mathbf{b}_i\left(\hat{u}_{i1}^{(n)}, \hat{v}_{i1}^{(n)}\right),\ldots,\mathbf{b}_i\left(\hat{u}_{iK}^{(n)}, \hat{v}_{iK}^{(n)}\right), \mathbf{b}_i\left(u_{\mathrm{I2I},i}^{\mathrm{A}}, v_{\mathrm{I2I},i}^{\mathrm{A}}\right)\right]. \tag{37}$$

Finally, the path loss $|\hat{\alpha}_{il}^{(n)}|$ corresponding to $(u_{il}^{(n)}, v_{il}^{(n)})$ is determined by the l-th diagonal element of $\hat{\mathbf{R}}_{\boldsymbol{\beta}_i}^{(n)}$.

2) Estimate All Possible Users' Locations and Their Corresponding Path Losses: By combining the estimated AoA pairs $(\hat{u}_{2l}^{(n)}, \hat{v}_{2l}^{(n)}) \in \mathcal{A}_2$ and $(\hat{u}_{2s}^{(n)}, \hat{v}_{2s}^{(n)}) \in \mathcal{A}_3$, we calculate the possible user location, which satisfies the following equations:

$$\hat{u}_{2l}^{(n)} = \frac{y_2 - \hat{y}_{\mathrm{U},ls}^{(n)}}{\hat{d}_{\mathrm{U2I},2,ls}^{(n)}},\ \hat{v}_{2l}^{(n)} = \frac{z_2 - \hat{z}_{\mathrm{U},ls}^{(n)}}{\hat{d}_{\mathrm{U2I},2,ls}^{(n)}}, \tag{38}$$

$$\hat{u}_{3s}^{(n)} = \frac{y_3 - \hat{y}_{\mathrm{U},ls}^{(n)}}{\hat{d}_{\mathrm{U2I},3,ls}^{(n)}},\ \hat{v}_{3s}^{(n)} = \frac{z_3 - \hat{z}_{\mathrm{U},ls}^{(n)}}{\hat{d}_{\mathrm{U2I},3,ls}^{(n)}}. \tag{39}$$

$$\mathbf{x}_i^{(n)}(t) = \sqrt{\rho}\,\alpha_{\mathrm{I2I},i}\mathbf{b}_i\left(u_{\mathrm{I2I},i}^{\mathrm{A}}, v_{\mathrm{I2I},i}^{\mathrm{A}}\right)\mathbf{b}_1^{\mathrm{H}}\left(u_{\mathrm{I2I},i}^{\mathrm{D}}, v_{\mathrm{I2I},i}^{\mathrm{D}}\right)\mathbf{\Theta}_1^{(n)}\sum_{k=1}^{K}\alpha_{\mathrm{U2I},1,k}\mathbf{b}_1\left(u_{\mathrm{U2I},1,k}^{\mathrm{A}}, v_{\mathrm{U2I},1,k}^{\mathrm{A}}\right)s_k(t)$$
$$+\sqrt{\rho}\sum_{k=1}^{K}\alpha_{\mathrm{U2I},i,k}\mathbf{b}_i\left(u_{\mathrm{U2I},i,k}^{\mathrm{A}}, v_{\mathrm{U2I},i,k}^{\mathrm{A}}\right)s_k(t) + \mathbf{n}_i(t),\ i=2,3,\ t\in\mathcal{N}_n,\ n=1,2, \tag{29}$$

Let $\hat{\mathbf{q}}_{\mathrm{U},ls}^{(n)} \triangleq [\hat{x}_{\mathrm{U},ls}^{(n)}, \hat{y}_{\mathrm{U},ls}^{(n)}, \hat{z}_{\mathrm{U},ls}^{(n)}]^{\mathrm{T}}$ and $\hat{d}_{\mathrm{U2I},i,ls}^{(n)} \triangleq \|\hat{\mathbf{q}}_{\mathrm{U},ls}^{(n)} - \mathbf{q}_i\|$. The above equations can be compactly expressed as

$$\hat{\mathbf{A}}_{ls}^{(n)} \hat{\mathbf{z}}_{ls}^{(n)} = \mathbf{p}, \tag{40}$$

where

$$\hat{\mathbf{A}}_{ls}^{(n)} \triangleq \begin{pmatrix} 1 & 0 & \hat{u}_{2l}^{(n)} & 0 \\ 0 & 1 & \hat{v}_{2l}^{(n)} & 0 \\ 1 & 0 & 0 & \hat{u}_{3s}^{(n)} \\ 0 & 1 & 0 & \hat{v}_{3s}^{(n)} \end{pmatrix}, \tag{41}$$

$$\hat{\mathbf{z}}_{ls}^{(n)} \triangleq \left[\hat{y}_{\mathrm{U},ls}^{(n)}, \hat{z}_{\mathrm{U},ls}^{(n)}, \hat{d}_{\mathrm{U2I},2,ls}^{(n)}, \hat{d}_{\mathrm{U2I},3,ls}^{(n)}\right]^{\mathrm{T}}, \tag{42}$$

$$\mathbf{p} \triangleq [y_2, z_2, y_3, z_3]^{\mathrm{T}}. \tag{43}$$

By solving the above matrix equation, we obtain

$$\hat{d}_{\mathrm{U2I},2,ls}^{(n)} = \frac{\hat{u}_{3s}^{(n)}(z_2 - z_3) - \hat{v}_{3s}^{(n)}(y_2 - y_3)}{\hat{u}_{3s}^{(n)}\hat{v}_{2l}^{(n)} - \hat{u}_{2l}^{(n)}\hat{v}_{3s}^{(n)}}, \tag{44}$$

$$\hat{d}_{\mathrm{U2I},3,ls}^{(n)} = \frac{\hat{u}_{2l}^{(n)}(z_3 - z_2) - \hat{v}_{2\,l}^{(n)}(y_3 - y_2)}{\hat{u}_{2l}^{(n)}\hat{v}_{3s}^{(n)} - \hat{u}_{3s}^{(n)}\hat{v}_{2l}^{(n)}}, \tag{45}$$

$$\hat{y}_{\mathrm{U},ls}^{(n)} = y_2 - \hat{u}_{2l}^{(n)}\hat{d}_{\mathrm{U2I},2,l}^{(n)}, \tag{46}$$

$$\hat{z}_{\mathrm{U},ls}^{(n)} = z_2 - \hat{v}_{2l}^{(n)}\hat{d}_{\mathrm{U2I},2,l}^{(n)}. \tag{47}$$

Next, we calculate $\hat{x}_{\mathrm{U},ls}^{(n)}$ according to the following equation

$$\left(\hat{x}_{\mathrm{U},ls}^{(n)} - x_i\right)^2 + \left(\hat{y}_{\mathrm{U},ls}^{(n)} - y_i\right)^2 + \left(\hat{z}_{\mathrm{U},ls}^{(n)} - z_i\right)^2 = \left(\hat{d}_{\mathrm{U2I},i,ls}^{(n)}\right)^2, i = 2, 3, \tag{48}$$

and obtain

$$\hat{x}_{\mathrm{U},ls}^{(n)} = \arg\min_{\omega_2} \min_{\omega_2 \in \{x_2 \pm d_{x,2,ls}\}, \omega_3 \in \{x_3 \pm d_{x,3,ls}\}} |\omega_2 - \omega_3|, \tag{49}$$

where $d_{x,i,ls} \triangleq \sqrt{(\hat{d}_{\mathrm{U2I},i,ls}^{(n)})^2 - (\hat{y}_{\mathrm{U},ls}^{(n)} - y_i)^2 - (\hat{z}_{\mathrm{U},ls}^{(n)} - z_i)^2}$.

Finally, by combining (46), (47) and (49), we estimate $\hat{\mathbf{q}}_{\mathrm{U},ls}^{(n)}$ and calculate the corresponding distance-dependent path loss according to the log-distance path loss model [35] as

$$\left|\breve{\alpha}_{i,ls}^{(n)}\right| = 10^{-\frac{1}{20}\left(PL(d_0) + 10\epsilon_{\mathrm{U2I}} \log\left(\frac{\left\|\hat{\mathbf{q}}_{\mathrm{U},ls}^{(n)} - \mathbf{q}_i\right\|}{d_0}\right)\right)}, \tag{50}$$

where d_0 is the reference distance, and ϵ_{U2I} is the path loss exponent from users to the IRS.

3) Simultaneous Multi-User Location Sensing Through AoA Matching: In order to match the effective AoA pairs in $\mathcal{A}_2$ with those in $\mathcal{A}_3$ so that they are corresponding to the same user, we propose an AoA matching algorithm.

For the effective AoA pair $(\hat{u}_{2l}^{(n)}, \hat{v}_{2l}^{(n)}) \in \mathcal{A}_2$, we denote its corresponding effective AoA pair in $\mathcal{A}_3$ by $(\hat{u}_{3sl}^{(n)}, \hat{v}_{3sl}^{(n)})$. Then, we initialize $\mathcal{S} = \{1, \ldots, K\}$ and estimate s_l in the l-th iteration as

$$\hat{s}_l = \arg\min_{s \in \mathcal{S}} \left| \left[\left|\breve{\alpha}_{2,ls}^{(n)}\right|, \left|\breve{\alpha}_{3,ls}^{(n)}\right|\right]^{\mathrm{T}} - \left[\left|\hat{\alpha}_{2l}^{(n)}\right|, \left|\hat{\alpha}_{3s}^{(n)}\right|\right]^{\mathrm{T}} \right|, \tag{51}$$

based on which, we obtain an estimated user location $\hat{\mathbf{q}}_{\mathrm{U},l\hat{s}_l}^{(n)}$, and remove $\hat{s}_l$ from $\mathcal{S}$. After K iterations, we obtain the locations of K users, i.e., $\mathcal{K}^{(n)} = \{\hat{\mathbf{q}}_{\mathrm{U},k}^{(n)}, k = 1, \ldots, K\}$. The detailed process of the AoA matching algorithm is provided in Algorithm 1.

Finally, we summarize in Algorithm 2 the main procedures of the proposed multi-user location sensing algorithm.

Remark 1: In addition to supporting localization services, the sensed users' locations can be used for improving communication performance through for example beamforming design.

Remark 2: There are four main contributions of the proposed location sensing algorithm. First, the proposed location sensing algorithm conducts user localization based on the communication signals, which means that communication and localization are conducted simultaneously, sharing the same time-frequency resources. While the conventional localization technique utilizes dedicated positioning reference signals to conduct multi-user

Algorithm 1: AoA Matching Algorithm.

Input: $|\hat{\alpha}_{il}^{(n)}|$, $|\breve{\alpha}_{i,ls}^{(n)}|$, $\hat{\mathbf{q}}_{\mathrm{U},ls}^{(n)}$.
1: Initialize $\mathcal{K}^{(n)} = \oslash$, $\mathcal{S} = \{1, \ldots, K\}$.
2: **for** $l = 1, \ldots, K$ **do**
3: Calculate $\hat{s}_l$ according to (51).
4: Add $\hat{\mathbf{q}}_{\mathrm{U},l\hat{s}_l}^{(n)}$ into $\mathcal{K}^{(n)}$.
5: Remove $\hat{s}_l$ from $\mathcal{S}$.
6: **end for**
Output: $\mathcal{K}^{(n)}$.

Algorithm 2: Multi-User Location Sensing Algorithm.

Input: $\mathbf{x}_i^{(n)}(t)$, $\mathbf{q}_i$.
1: Estimate the effective AoA pairs corresponding to the links from the K users to the two semi-passive sub-IRSs according to Section III-A, which yields $\mathcal{A}_i, i = 2, 3$.
2: Estimate the path losses corresponding to the effective AoA pairs in $\mathcal{A}_i, i = 2, 3$ according to Section III-B.1), which yields $|\hat{\alpha}_{il}^{(n)}|, l = 1, \ldots, K, i = 2, 3$.
3: Estimate all possible users' locations and their corresponding path losses according to Section III-B.2), which yields $\hat{q}_{\mathrm{U},ls}^{(n)}$ and $|\breve{\alpha}_{i,ls}^{(n)}|, l, s = 1, \ldots, K, i = 2, 3$.
4: Determine users' locations $\mathcal{K}^{(n)}$ based on Algorithm 1.
Output: $\mathcal{K}^{(n)}$.

$$\hat{\mathbf{R}}_{\boldsymbol{\beta}_i}^{(n)} = \frac{1}{\rho}\left(\left[\hat{\mathbf{B}}_i^{(n)}\right]^{\mathrm{H}}\hat{\mathbf{B}}_i^{(n)}\right)^{-1}\left[\hat{\mathbf{B}}_i^{(n)}\right]^{\mathrm{H}}\left(\hat{\mathbf{R}}_i^{(n)} - \sigma_0^2\mathbf{I}\right)\hat{\mathbf{B}}_i^{(n)}\left(\left[\hat{\mathbf{B}}_i^{(n)}\right]^{\mathrm{H}}\hat{\mathbf{B}}_i^{(n)}\right)^{-1} \tag{35}$$

localization on orthogonal time-frequency resources. Second, for the uniform rectangular array, using the MUSIC technique requires the exhaustive search for AoAs in a two-dimensional plane. To avoid the high complexity, we combine the use of the TLS-ESPRIT and MUSIC techniques such that the AOAs can be searched only within a $(K+1)^2$-element set. Third, during the ISAC period, the semi-passive sub-IRS suffers interference from the reflection of the passive sub-IRS. Note that such interference issue is caused by the new IRS architecture, and does not exist in the traditional location sensing. To eliminate this interference, an effective interference cancellation method is proposed. Fourth, in order to estimate multiple users' locations simultaneously, we propose an AoA matching algorithm such that multiple users' locations can be estimated on the same time-frequency resources. While most existing AoA-based location sensing algorithms consider that multiple users' locations are estimated on orthogonal time-frequency resources.

IV. Sensing-Based Joint Active and Passive Beamforming

In this section, we propose two sensing-based beamforming algorithms to maximize the sum rate for the ISAC and PC periods, respectively, by capitalizing on the users' locations sensed in the ISAC period.

A. ISAC Period

In the ISAC period, we first design the BS combining vectors by adopting the maximum ratio combining (MRC) technique, and then propose an estimation of distribution algorithm (EDA) based beamforming method to optimize the phase shift matrix of the passive sub-IRS.

During the n-th time block of the ISAC period, the sum rate of K users is given by

$$R_{\text{sum}}\left(\mathbf{W}^{(n)},\mathbf{\Theta}_1^{(n)}\right)= \sum_{k=1}^{K}\log_2\left(1+\frac{\rho\left|\left[\mathbf{w}_k^{(n)}\right]^{\text{H}}\mathbf{H}_{\text{I2B},1}\mathbf{\Theta}_1^{(n)}\mathbf{h}_{\text{U2I},1,k}^{(n)}\right|^2}{\rho\sum_{j\neq k}^{K}\left|\left[\mathbf{w}_k^{(n)}\right]^{H}\mathbf{H}_{\text{I2B},1}\mathbf{\Theta}_1^{(n)}\mathbf{h}_{\text{U2I},1,j}^{(n)}\right|^2+\sigma_0^2}\right), \tag{52}$$

where the combining matrix $\mathbf{W}^{(n)}$ is defined as $\mathbf{W}^{(n)}\triangleq[\mathbf{w}_1^{(n)},\ldots,\mathbf{w}_K^{(n)}]$. As such, the sum rate maximization problem is formulated as

$$(\text{P1}):\max_{\mathbf{W}^{(n)},\mathbf{\Theta}_1^{(n)}}\ R_{\text{sum}}\left(\mathbf{W}^{(n)},\mathbf{\Theta}_1^{(n)}\right), \tag{53a}$$

$$\text{s.t.}\quad \left\|\mathbf{w}_k^{(n)}\right\|=1, \tag{53b}$$

$$\vartheta_{1,m}^{(n)}\in\mathcal{F}_b, m=1,\ldots,M_1. \tag{53c}$$

1) BS Combining Vectors Optimization: With the given phase shift matrix $\mathbf{\Theta}_1^{(n)}$, the problem (P1) can be reduced to the optimization of $\mathbf{W}^{(n)}$. By adopting the MRC technique, we obtain the combining vector for the k-th user as

$$\mathbf{w}_k^{(n)}=\frac{\mathbf{H}_{\text{I2B},1}\mathbf{\Theta}_1^{(n)}\mathbf{h}_{\text{U2I},1,k}^{(n)}}{\left\|\mathbf{H}_{\text{I2B},1}\mathbf{\Theta}_1^{(n)}\mathbf{h}_{\text{U2I},1,k}^{(n)}\right\|}. \tag{54}$$

Since the locations of the BS and all the sub-IRSs are fixed, we consider that $\mathbf{H}_{\text{I2B},i}$ is perfectly known [36]. Although $\mathbf{h}_{\text{U2I},i,k}^{(n)}$ is unavailable due to the phase ambiguity of its complex channel gain $\alpha_{\text{U2I},i,k}$, this phase ambiguity would not affect the calculation of R_{sum}. Therefore, we define $\mathbf{h}_{\text{abs},i,k}^{(n)}\triangleq|\alpha_{\text{U2I},i,k}^{(n)}|\mathbf{b}_i(u_{\text{U2I},i,k}^{\text{A},(n)},v_{\text{U2I},i,k}^{\text{A},(n)})$, and design $\mathbf{w}_k^{(n)}$ as (55) shown at the bottom of the next page. Due to $\|\mathbf{w}_k^{(n)}\|=1$, (56) shown at the bottom of the next page, can be easily verified. Substituting (56) into (55) yields $\mathbf{w}_k^{(n)}=\frac{1}{N}\mathbf{a}(u_{\text{I2B},1}^{\text{A}})$. Therefore, for any $\mathbf{\Theta}_1^{(n)}$, we obtain $\mathbf{W}^{(n)}$ as

$$\mathbf{W}^{(n)}=\frac{1}{N}\left[\mathbf{a}\left(u_{\text{I2B},1}^{\text{A}}\right),\ldots,\mathbf{a}\left(u_{\text{I2B},1}^{\text{A}}\right)\right]\in\mathbb{C}^{N\times K}. \tag{57}$$

2) IRS Phase Shift Matrix Optimization: With the given combining matrix $\mathbf{W}^{(n)}$, the problem (P1) can be simplified to the optimization of $\mathbf{\Theta}_1^{(n)}$. Since the user location information is unavailable in the first time block, $\mathbf{\Theta}_1^{(1)}$ is randomly generated. Therefore, in the following, we only focus on the design of $\mathbf{\Theta}_1^{(2)}$ in the second time block by invoking the users' locations sensed in the first time block.

First, we set the probability matrix corresponding to $\mathbf{\Theta}_1^{(2)}$ as $\mathbf{P}_1^{(2)}=[\mathbf{p}_{1,1}^{(2)},\ldots,\mathbf{p}_{1,m}^{(2)},\ldots,\mathbf{p}_{1,M_1}^{(2)}]\in\mathbb{C}^{2^b\times M_1}$, where $\mathbf{p}_{1,m}^{(2)}=[p_{1,m,1}^{(2)},\ldots,p_{1,m,2^b}^{(2)}]^{\text{T}}$ denotes the probability parameter for $\vartheta_{1,m}^{(2)}$, with its entry $p_{1,m,l}^{(2)}$ satisfying the probability constraints $0\leqslant p_{1,m,l}^{(2)}\leqslant 1$ and $\sum_{l=1}^{2^b}p_{1,m,l}^{(2)}=1$. Subsequently, we consider that $\vartheta_{1,m}^{(2)}$ takes a value from $\mathcal{F}_b$ with an equal probability at first, and initialize the probability matrix as $\mathbf{P}_1^{(2),0}=\frac{1}{2^b}\times\mathbf{1}_{2^b\times M_1}$. Then, in the i-th iteration, we randomly generate S_{ISAC} candidates $\{\mathbf{\Theta}_1^{(2),s}\}_{s=1}^{S_{\text{ISAC}}}$ according to the probability distribution function given by

$$\Xi\left(\mathbf{\Theta}_1^{(2)};\mathbf{P}_1^{(2),i}\right)=\prod_{m=1}^{M_1}\left(\left(\prod_{l=1}^{2^b-1}\left(p_{1,m,l}^{(2),i}\right)^{\Gamma\left(\vartheta_{1,m}^{(2)},\mathcal{F}_b(l)\right)}\right)\times\left(1-\prod_{l=1}^{2^b-1}\left(p_{1,m,l}^{(2),i}\right)^{\Gamma\left(\vartheta_{1,m}^{(2)},\mathcal{F}_b(l)\right)}\right)\right), \tag{58}$$

where $\mathcal{F}_b(l)$ denotes the l-th entry of $\mathcal{F}_b$, and $\Gamma(\vartheta_{1,m}^{(2)},\mathcal{F}_b(l))$ is a judge function given by

$$\Gamma\left(\vartheta_{1,m}^{(2)},\mathcal{F}_b(l)\right)=\begin{cases}1,\vartheta_{1,m}^{(2)}=\mathcal{F}_b(l)\\0,\vartheta_{1,m}^{(2)}\neq\mathcal{F}_b(l)\end{cases}. \tag{59}$$

For each phase shift matrix candidate $\mathbf{\Theta}_1^{(2),s}$, we calculate the corresponding sum rate

$$R_{\text{sum}}\left(\mathbf{\Theta}_1^{(2),s}\right)$$

$$=\sum_{k=1}^{K}\log_2\left(1+\frac{\rho\left|\left[\mathbf{w}_k^{(2)}\right]^{\mathrm{H}}\mathbf{H}_{\mathrm{I2B},1}\boldsymbol{\Theta}_1^{(2),s}\hat{\mathbf{h}}_{\mathrm{abs},1,k}^{(1)}\right|^2}{\rho\sum_{j\neq k}^{K}\left|\left[\mathbf{w}_k^{(2)}\right]^{\mathrm{H}}\mathbf{H}_{\mathrm{I2B},1}\boldsymbol{\Theta}_1^{(2),s}\hat{\mathbf{h}}_{\mathrm{abs},1,j}^{(1)}\right|^2+\sigma_0^2}\right), \tag{60}$$

where

$$\hat{\mathbf{h}}_{\mathrm{abs},1,k}^{(n)}=\left|\hat{\alpha}_{\mathrm{U2I},1,k}^{(n)}\right|\mathbf{b}_1\left(\hat{u}_{\mathrm{U2I},1,k}^{\mathrm{A},(n)},\hat{v}_{\mathrm{U2I},1,k}^{\mathrm{A},(n)}\right),n=1,2, \tag{61}$$

$$\hat{u}_{\mathrm{U2I},1,k}^{\mathrm{A},(n)}=\frac{\hat{y}_{\mathrm{U},k}^{(n)}-y_1}{\parallel\hat{\mathbf{q}}_{\mathrm{U},k}^{(n)}-\mathbf{q}_1\parallel},\hat{v}_{\mathrm{U2I},1,k}^{\mathrm{A},(n)}=\frac{\hat{z}_{\mathrm{U},k}^{(n)}-z_1}{\parallel\hat{\mathbf{q}}_{\mathrm{U},k}^{(n)}-\mathbf{q}_1\parallel}, \tag{62}$$

$$\left|\hat{\alpha}_{\mathrm{U2I},1,k}^{(n)}\right|=10^{-\frac{1}{20}\left(PL(d_0)+10\epsilon_{\mathrm{U2I}}\log\left(\frac{\left\|\hat{\mathbf{q}}_{\mathrm{U},k}^{(n)}-\mathbf{q}_1\right\|}{d_0}\right)\right)}. \tag{63}$$

After that, we sort $\mathcal{R}_{\mathrm{ISAC}}=\{R_{\mathrm{sum}}(\boldsymbol{\Theta}_1^{(2),s})\}_{s=1}^{S_{\mathrm{ISAC}}}$ in descending order and select the $S_{\mathrm{ISAC}}^{\mathrm{elite}}$ phase shift matrix samples corresponding to the $S_{\mathrm{ISAC}}^{\mathrm{elite}}$ largest sum rates in $\mathcal{R}_{\mathrm{ISAC}}$, i.e., $\boldsymbol{\Theta}_1^{(2),s_q}, s_q=1,\ldots,S_{\mathrm{ISAC}}^{\mathrm{elite}}$. Based on the selected $S_{\mathrm{ISAC}}^{\mathrm{elite}}$ samples, we update the probability matrix in the $(i+1)$-th iteration as $\mathbf{P}_1^{(2),i+1}$ with its elements given by

$$p_{1,m,l}^{(2),i+1}=\frac{1}{S_{\mathrm{ISAC}}^{\mathrm{elite}}}\sum_{s_q=1}^{S_{\mathrm{ISAC}}^{\mathrm{elite}}}\Gamma\left(\vartheta_{1,m}^{(2),s_q},\mathcal{F}_b(l)\right),$$
$$m=1,\ldots,M_1,\ l=1,\ldots,2^b. \tag{64}$$

Repeat the above process until the difference between the maximum and minimum of $\mathcal{R}_{\mathrm{ISAC}}$ is less than the threshold κ, which indicates that $\mathbf{P}_1^{(2)}$ is stable. The procedures of the beamforming algorithm in the second time block of the ISAC period are summarized in Algorithm 3.

Algorithm 3: Sensing-Based Beamforming for the Second Time Block of the ISAC Period.

Input: $\mathcal{K}^{(1)}$, $\mathbf{H}_{\mathrm{I2B},1}$, S_{ISAC}, $S_{\mathrm{ISAC}}^{\mathrm{elite}}$, $\mathcal{F}_b$.

1: Initialize $\mathbf{P}_1^{(2),0}=\frac{1}{2^b}\times\mathbf{1}_{2^b\times M_1}$, and $i=1$.
2: Calculate $\mathbf{W}^{(2)}$ based on the MRC method.
3: **repeat**
4: Randomly generate S_{ISAC} candidates $\{\boldsymbol{\Theta}_1^{(2),s}\}_{s=1}^{S_{\mathrm{ISAC}}}$ based on $\Xi(\boldsymbol{\Theta}_1^{(2)};\mathbf{P}_1^{(2),i})$.
5: Calculate the sum rate $\{R_{\mathrm{sum}}(\boldsymbol{\Theta}_1^{(2),s})\}_{s=1}^{S_{\mathrm{ISAC}}}$ by (60).
6: Sort $\mathcal{R}_{\mathrm{ISAC}}=\{R_{\mathrm{sum}}(\boldsymbol{\Theta}_1^{(2),s})\}_{s=1}^{S_{\mathrm{ISAC}}}$ in descending order.
7: Select $S_{\mathrm{ISAC}}^{\mathrm{elite}}$ phase shift matrix samples corresponding to the $S_{\mathrm{ISAC}}^{\mathrm{elite}}$ largest sum rates in $\mathcal{R}_{\mathrm{ISAC}}$.
8: Update $\mathbf{P}_1^{(2),i+1}$ according to (64).
9: Let $i\rightarrow i+1$.
10: **until** $|\max(\mathcal{R}_{\mathrm{ISAC}})-\min(\mathcal{R}_{\mathrm{ISAC}})|<\kappa$

Output: $\boldsymbol{\Theta}_1^{(2),\mathrm{opt}}=\mathrm{diag}(\boldsymbol{\xi}_1^{(2),\mathrm{opt}})=\boldsymbol{\Theta}_1^{(2),1}$, $\mathbf{W}^{(2),\mathrm{opt}}=\mathbf{W}^{(2)}$.

B. PC Period

During the PC period, all three sub-IRSs operate in the reflecting mode to assist uplink transmission, and the sum rate of K users can be expressed as

$$R_{\mathrm{sum}}\left(\mathbf{W}(t),\boldsymbol{\Theta}(t)\right)$$
$$=\sum_{k=1}^{K}\log_2\left(1+\frac{\rho\left|\mathbf{w}_k^{\mathrm{H}}(t)\mathbf{H}_{\mathrm{I2B}}\boldsymbol{\Theta}(t)\mathbf{h}_{\mathrm{U2I},k}\right|^2}{\rho\sum_{j\neq k}^{K}\left|\mathbf{w}_k^{\mathrm{H}}(t)\mathbf{H}_{\mathrm{I2B}}\boldsymbol{\Theta}(t)\mathbf{h}_{\mathrm{U2I},j}\right|^2+\sigma_0^2}\right),$$
$$t\in\mathcal{T}_2, \tag{65}$$

where $\mathbf{W}(t)$ is defined as $\mathbf{W}(t)\triangleq[\mathbf{w}_1(t),\ldots,\mathbf{w}_K(t)]$. As such, the sum rate maximization problem is formulated as

$$(\mathrm{P2}):\max_{\mathbf{W}(\mathrm{t}),\boldsymbol{\Theta}(\mathrm{t})}\ R_{\mathrm{sum}}\left(\mathbf{W}(t),\boldsymbol{\Theta}(t)\right), \tag{66a}$$
$$\mathrm{s.t.}\quad\|\mathbf{w}_k(t)\|=1, \tag{66b}$$
$$\vartheta_{i,m}(t)\in\mathcal{F}_b,m=1,\ldots,M_i,i=1,2,3. \tag{66c}$$

Note that the calculation of the sum rate involves $\mathbf{h}_{\mathrm{U2I},k}$, which is unavailable due to the phase ambiguity of $\alpha_{\mathrm{U2I},i,k}$. Hence, during the first C time slots of the PC period ($C\ll T_2$), we set $\mathbf{W}(t)=\mathbf{W}^{(2),\mathrm{opt}}$ and $\boldsymbol{\Theta}(t)=\mathrm{diag}(\boldsymbol{\xi}(t))$ in time slot $t\in\mathcal{T}_{\mathrm{c}}\triangleq\{T_1+1,\ldots,T_1+C\}$, where $\boldsymbol{\xi}(t)=[[\boldsymbol{\xi}_1^{(2),\mathrm{opt}}]^{\mathrm{T}},[\boldsymbol{\xi}_2(t)]^{\mathrm{T}},[\boldsymbol{\xi}_3(t)]^{\mathrm{T}}]^{\mathrm{T}}$, and $\boldsymbol{\xi}_i(t)$ is randomly generated phase shift beam of the i-th ($i=2,3$) sub-IRS.

With the received signal strength obtained in the first C time slots of the PC period and the users' locations estimated in the ISAC period, the phase ambiguity of $\alpha_{\mathrm{U2I},i,k}$ can be removed, which enables the sum rate calculation in the remaining time slots of the PC period. As such, in the remaining time slots of the PC period, we propose a joint active and passive beamforming algorithm to solve the sum rate maximization problem (P2), by combining the use of zero-forcing (ZF) and EDA-based techniques.

$$\mathbf{w}_k^{(n)}=\frac{\mathbf{H}_{\mathrm{I2B},1}\boldsymbol{\Theta}_1^{(n)}\mathbf{h}_{\mathrm{abs},1,k}^{(n)}}{\left\|\mathbf{H}_{\mathrm{I2B},1}\boldsymbol{\Theta}_1^{(n)}\mathbf{h}_{\mathrm{abs},1,k}^{(n)}\right\|}=\frac{\alpha_{\mathrm{I2B},1}\mathbf{a}\left(u_{\mathrm{I2B},1}^{\mathrm{A}}\right)\mathbf{b}_1^{\mathrm{H}}\left(u_{\mathrm{I2B},1}^{\mathrm{D}},v_{\mathrm{I2B},1}^{\mathrm{D}}\right)\boldsymbol{\Theta}_1^{(n)}\left|\alpha_{\mathrm{U2I},1,k}^{(n)}\right|\mathbf{b}_1\left(u_{\mathrm{U2I},1,k}^{\mathrm{A},(n)},v_{\mathrm{U2I},1,k}^{\mathrm{A},(n)}\right)}{\left\|\mathbf{H}_{\mathrm{I2B},1}\boldsymbol{\Theta}_1^{(n)}\mathbf{h}_{\mathrm{abs},1,k}^{(n)}\right\|} \tag{55}$$

$$\frac{\alpha_{\mathrm{I2B},1}\mathbf{b}_1^{\mathrm{H}}\left(u_{\mathrm{I2B},1}^{\mathrm{D}},v_{\mathrm{I2B},1}^{\mathrm{D}}\right)\boldsymbol{\Theta}_1^{(n)}\left|\alpha_{\mathrm{U2I},1,k}^{(n)}\right|\mathbf{b}_1\left(u_{\mathrm{U2I},1,k}^{\mathrm{A},(n)},v_{\mathrm{U2I},1,k}^{\mathrm{A},(n)}\right)}{\left\|\mathbf{H}_{\mathrm{I2B},1}\boldsymbol{\Theta}_1^{(n)}\mathbf{h}_{\mathrm{abs},1,k}^{(n)}\right\|}=\frac{1}{N} \tag{56}$$

1) Remove the Phase Ambiguity of $\alpha_{U2I,i,k}$: We first reformulate $\mathbf{h}_{\mathrm{U2I},k}$ as

$$\begin{aligned}\mathbf{h}_{\mathrm{U2I},k} &= \left[e^{j\psi_{1,k}}\mathbf{h}_{\mathrm{abs},1,k}^{\mathrm{T}},\ e^{j\psi_{2,k}}\mathbf{h}_{\mathrm{abs},2,k}^{\mathrm{T}},\ e^{j\psi_{3,k}}\mathbf{h}_{\mathrm{abs},3,k}^{\mathrm{T}}\right]^{\mathrm{T}}\\ &= e^{j\psi_{1,k}}\left[\mathbf{h}_{\mathrm{abs},1,k}^{\mathrm{T}},\ e^{j(\psi_{2,k}-\psi_{1,k})}\mathbf{h}_{\mathrm{abs},2,k}^{\mathrm{T}},\ e^{j(\psi_{3,k}-\psi_{1,k})}\mathbf{h}_{\mathrm{abs},3,k}^{\mathrm{T}}\right]^{\mathrm{T}}\\ &= e^{j\psi_{1,k}}\left[\mathbf{h}_{\mathrm{abs},1,k}^{\mathrm{T}},\ e^{j\Delta_{2,k}}\mathbf{h}_{\mathrm{abs},2,k}^{\mathrm{T}},\ e^{j\Delta_{3,k}}\mathbf{h}_{\mathrm{abs},3,k}^{\mathrm{T}}\right]^{\mathrm{T}},\end{aligned} \tag{67}$$

where $\mathbf{h}_{\mathrm{abs},i,k} \triangleq |\alpha_{\mathrm{U2I},i,k}|\mathbf{b}_i(u_{\mathrm{U2I},i,k}^{\mathrm{A}}, v_{\mathrm{U2I},i,k}^{\mathrm{A}})$ and $\psi_{i,k}$ denotes the phase of $\alpha_{\mathrm{U2I},i,k}$. In the following, we try to estimate $\Delta_{i,k}$ ($i \in \{2,3\}$ and $k \in \{1,\ldots,K\}$), by exploiting the BS received signal strength obtained during the first C time slots of the PC period. Define

$$\mathbf{D} \triangleq \begin{bmatrix} \Delta_{2,1},\ldots,\Delta_{2,k},\ldots,\Delta_{2,K} \\ \Delta_{3,1},\ldots,\Delta_{3,k},\ldots,\Delta_{3,K} \end{bmatrix}, \tag{68}$$

and assume that $\Delta_{i,k}$ belongs to the set $\mathcal{F}_\Delta = \left\{0, \frac{2\pi}{2^{b_\Delta}},\ldots,\frac{2\pi}{2^{b_\Delta}}(2^{b_\Delta}-1)\right\}$, where b_Δ is the bit-quantization number, and $\Delta_{i,k}$ is approximately a continuous phase shift when b_Δ is sufficiently large. Based on this assumption, $\mathbf{D}$ has 4^{Kb_Δ} possible values (i.e., $\mathcal{D} \triangleq \{\mathbf{D} \,|\, \Delta_{i,k} \in \mathcal{F}_\Delta, i = 2,3, k = 1,\ldots,K\}$). For each possible value $\check{\mathbf{D}} \in \mathcal{D}$, the corresponding BS received signal strength in time slot $t \in \mathcal{T}_{\mathrm{c}}$ can be calculated as

$$\begin{aligned}\check{P}\left(\check{\mathbf{D}}, \boldsymbol{\Theta}(t)\right) = \sum_{k=1}^{K}\left(\rho\left|\mathbf{w}_k^{\mathrm{H}}(t)\mathbf{H}_{\mathrm{I2B}}\boldsymbol{\Theta}(t)\check{\mathbf{h}}_{\Delta,k}\right|^2\right)\\ + \sigma_0^2, t \in \mathcal{T}_{\mathrm{c}},\end{aligned} \tag{69}$$

where $\check{\mathbf{h}}_{\Delta,k} = [[\hat{\mathbf{h}}_{\mathrm{abs},1,k}^{(2)}]^{\mathrm{T}}, e^{j\check{\Delta}_{2,k}}[\hat{\mathbf{h}}_{\mathrm{abs},2,k}^{(2)}]^{\mathrm{T}}, e^{j\check{\Delta}_{3,k}}[\hat{\mathbf{h}}_{\mathrm{abs},3,k}^{(2)}]^{\mathrm{T}}]^{\mathrm{T}}$.

Then, compare the possible BS received signal strength $\check{P}(\check{\mathbf{D}}, \boldsymbol{\Theta}(t))$ with the BS received signal strength $P(\boldsymbol{\Theta}(t))$ obtained during the first C time slots of the PC period, and define

$$f\left(\check{\mathbf{D}}\right) \triangleq \sum_{t\in\mathcal{T}_{\mathrm{c}}}\left|\check{P}\left(\check{\mathbf{D}}, \boldsymbol{\Theta}(t)\right) - P\left(\boldsymbol{\Theta}(t)\right)\right|. \tag{70}$$

As such, $\Delta_{i,k}$ can be estimated as

$$\hat{\Delta}_{i,k} = \left[\arg\min_{\check{\mathbf{D}}\in\mathcal{D}} f\left(\check{\mathbf{D}}\right)\right]_{(i-1)k}, i = 2,3,\ k = 1,\ldots,K. \tag{71}$$

2) Joint Active and Passive Beamforming: First, we set the probability matrix corresponding to $\boldsymbol{\Theta}(t)$ as $\mathbf{P} = [\mathbf{p}_1,\ldots,\mathbf{p}_m,\ldots,\mathbf{p}_M] \in \mathbb{C}^{2^b\times M}$, where $\mathbf{p}_m = [p_{m,1},\ldots,p_{m,2^b}]^{\mathrm{T}}$ denotes the probability parameter for ϑ_m, with its entry $p_{m,l}$ satisfying the probability constraints $0 \leqslant p_{m,l} \leqslant 1$ and $\sum_{l=1}^{2^b} p_{m,l} = 1$. Subsequently, before the first iteration, we consider that ϑ_m takes a value from $\mathcal{F}_b$ with an equal probability, and initialize $\mathbf{P}^0 = \frac{1}{2^b} \times \mathbf{1}_{2^b\times M}$. Then, in the i-th iteration, we randomly generate S_{PC} candidates $\{\boldsymbol{\Theta}^s(t)\}_{s=1}^{S_{\mathrm{PC}}}$ according to the probability distribution function given by

$$\Xi\left(\boldsymbol{\Theta}(t); \mathbf{P}^i\right) = \prod_{m=1}^{M}\left(\left(\prod_{l=1}^{2^b-1}\left(p_{m,l}^i\right)^{\Gamma(\vartheta_m(t),\mathcal{F}_b(l))}\right) \times \left(1 - \prod_{l=1}^{2^b-1}\left(p_{m,l}^i\right)^{\Gamma(\vartheta_m(t),\mathcal{F}_b(l))}\right)\right). \tag{72}$$

For each $\boldsymbol{\Theta}^s(t)$, we define the corresponding effective channel as $\mathbf{H}_{\mathrm{eq}}^s \triangleq \mathbf{H}_{\mathrm{I2B}}\boldsymbol{\Theta}^s(t)\hat{\mathbf{H}}_\Delta \in \mathbb{C}^{N\times K}$, where

$$\hat{\mathbf{H}}_\Delta = \left[\hat{\mathbf{h}}_{\Delta,1},\ldots,\hat{\mathbf{h}}_{\Delta,k},\ldots,\hat{\mathbf{h}}_{\Delta,K}\right], \tag{73}$$

$$\hat{\mathbf{h}}_{\Delta,k} = \left[\left[\hat{\mathbf{h}}_{\mathrm{abs},1,k}^{(2)}\right]^{\mathrm{T}}, e^{j\hat{\Delta}_{2,k}}\left[\hat{\mathbf{h}}_{\mathrm{abs},2,k}^{(2)}\right]^{\mathrm{T}}, e^{j\hat{\Delta}_{3,k}}\left[\hat{\mathbf{h}}_{\mathrm{abs},3,k}^{(2)}\right]^{\mathrm{T}}\right]^{\mathrm{T}}. \tag{74}$$

Then, following the ZF technique, we compute

$$\check{\mathbf{W}}^s(t) \triangleq [\check{\mathbf{w}}_1^s(t),\ldots,\check{\mathbf{w}}_K^s(t)] = \left[\left[\mathbf{H}_{\mathrm{eq}}^s\right]^{\mathrm{T}}\right]^{\dagger} \in \mathbb{C}^{N\times K}, \tag{75}$$

based on which, the combining vector for the k-th user is calculated as

$$\mathbf{w}_k^s(t) = \frac{\check{\mathbf{w}}_k^s(t)}{\|\check{\mathbf{w}}_k^s(t)\|}. \tag{76}$$

As such, the sum rate for each phase shift matrix candidate $\boldsymbol{\Theta}^s(t)$ can be calculated as

$$\begin{aligned}&R_{\mathrm{sum}}\left(\boldsymbol{\Theta}^s(t)\right)\\ &= \sum_{k=1}^{K}\log_2\left(1 + \frac{\rho\left|\left[\mathbf{w}_k^s(t)\right]^{\mathrm{H}}\mathbf{H}_{\mathrm{I2B}}\boldsymbol{\Theta}^s(t)\hat{\mathbf{h}}_{\Delta,k}\right|^2}{\rho\sum_{j\neq k}^{K}\left|\left[\mathbf{w}_k^s(t)\right]^{\mathrm{H}}\mathbf{H}_{\mathrm{I2B}}\boldsymbol{\Theta}^s(t)\hat{\mathbf{h}}_{\Delta,j}\right|^2 + \sigma_0^2}\right).\end{aligned} \tag{77}$$

Next, we sort $\mathcal{R}_{\mathrm{PC}} = \{R_{\mathrm{sum}}(\boldsymbol{\Theta}^s(t))\}_{s=1}^{S_{\mathrm{PC}}}$ in descending order and select $S_{\mathrm{PC}}^{\mathrm{elite}}$ phase shift matrix samples corresponding to the $S_{\mathrm{PC}}^{\mathrm{elite}}$ largest sum rates in $\mathcal{R}_{\mathrm{PC}}$, i.e., $\boldsymbol{\Theta}^{s_q}, s_q = 1,\ldots,S_{\mathrm{PC}}^{\mathrm{elite}}$. Based on the selected $S_{\mathrm{PC}}^{\mathrm{elite}}$ samples, we update the probability matrix in the $(i+1)$-th iteration as $\mathbf{P}^{i+1}$ with its elements given by

$$\begin{aligned}p_{m,l}^{i+1} = \frac{1}{S_{\mathrm{PC}}^{\mathrm{elite}}}\sum_{s_q=1}^{S_{\mathrm{PC}}^{\mathrm{elite}}}\Gamma\left(\vartheta_m^{s_q}(t), \mathcal{F}_b(l)\right),\\ m = 1,\ldots,M,\ l = 1,\ldots,2^b.\end{aligned} \tag{78}$$

Repeat the above process until the difference between the maximum and minimum of $\mathcal{R}_{\mathrm{PC}}$ is less than the threshold κ. The detailed process of the beamforming algorithm in the PC period is given by Algorithm 4.

Complexity analysis: The computational complexity of Algorithm 3/Algorithm 4 is mainly determined by the calculation of (60)/(77) and the number of generated candidates per iteration. As such, the complexity of Algorithm 3 and Algorithm 4 are $\mathcal{O}(K^2 {M_1}^2 N S_{\mathrm{ISAC}})$ and $\mathcal{O}(K^2\ M^2 N S_{\mathrm{PC}})$, respectively.

Convergence analysis: The proposed two beamforming algorithms are based on the EDA method, which has been proven in [37] to converge when $b = 1$. For $b > 1$, it is difficult to theoretically prove its convergence. In this case, we will provide some simulation results in the latter section to verify the convergence of the proposed beamforming algorithms.

Algorithm 4: Sensing-Based Beamforming Algorithm for the PC Period.

Input: $\mathcal{K}^{(2)}$, $\mathbf{H}_{\mathrm{I2B}}$, S_{PC}, $S_{\mathrm{PC}}^{\mathrm{elite}}$, $\mathcal{F}_b$.

1: Initialize $\mathbf{P}^0 = \frac{1}{2^b} \times \mathbf{1}_{2^b \times M}$, and $i = 1$.
2: Estimate $\Delta_{i,k}$ according to (71).
3: **repeat**
4: Randomly generate S_{PC} candidates $\{\mathbf{\Theta}^s(t)\}_{s=1}^{S_{\mathrm{PC}}}$ based on $\Xi(\mathbf{\Theta}(t); \mathbf{P}^i)$.
5: Calculate $\mathbf{W}^s(t)$ based on the ZF method.
6: Calculate the sum rate $\{R_{\mathrm{sum}}(\mathbf{\Theta}^s(t))\}_{s=1}^{S_{\mathrm{PC}}}$ by (77).
7: Sort $\mathcal{R}_{\mathrm{PC}} = \{R_{\mathrm{sum}}(\mathbf{\Theta}^s(t))\}_{s=1}^{S_{\mathrm{PC}}}$ in descending order.
8: Select $S_{\mathrm{PC}}^{\mathrm{elite}}$ phase shift matrix samples corresponding to the $S_{\mathrm{PC}}^{\mathrm{elite}}$ largest sum rate in $\mathcal{R}_{\mathrm{PC}}$.
9: Update $\mathbf{P}^{i+1}$ based on (78).
10: Let $i \to i+1$.
11: **until** $|\max(\mathcal{R}_{\mathrm{PC}}) - \min(\mathcal{R}_{\mathrm{PC}})| < \kappa$

Output: $\mathbf{\Theta}^{\mathrm{opt}}(t) = \mathbf{\Theta}^1(t)$, $\mathbf{W}^{\mathrm{opt}}(t) = \mathbf{W}^1(t)$

Remark 3: It is worth noting that the proposed two beamforming algorithms for both ISAC and PC periods are based on sensed location information instead of perfect CSI, which avoids high channel estimation overhead in the IRS-aided system.

V. Extension to the General Multi-IRS Case

The proposed IRS-enabled multi-user ISAC system can be extended to the general case with A passive sub-IRSs and B semi-passive sub-IRSs where $A \geqslant 1$ and $B \geqslant 2$. For localization, during the ISAC period, by utilizing the proposed AoA estimation scheme in Section III-A, the effective AoA pairs corresponding to multiple users can be estimated at B semi-passive sub-IRSs. Then, with the $B \times K$ pairs of effective AoAs, we combine the path loss estimation method and the AoA matching algorithm in Section III-B with the least square estimation technique such that the $B \times K$ pairs of effective AoAs can be fully used to achieve a high positioning accuracy. For communication, in both the ISAC and PC periods, by exploiting the sensed users' locations, we combine the use of ZF and EDA techniques (see Section IV-B) to design the joint active and passive beamforming such that better communication performance can be achieved.

VI. Simulation Results

In this section, numerical results are provided to demonstrate the effectiveness of the proposed multi-user location sensing and joint beamforming algorithms as well as to investigate the performance of the IRS-enabled multi-user ISAC system. The simulation setup is shown in Fig. 5, where K users are distributed on a ninety-degree sector of the horizontal floor. The BS is 20 meters (m) above the horizontal floor, and the three sub-IRSs are respectively 5 m, 7 m, and 9 m above the horizontal floor. The distances from the BS to the second sub-IRS and from the second sub-IRS to the users are set to be $d_{\mathrm{B2I},2} = 50$ m and $d_{\mathrm{I2U},2} = 10$ m, respectively. The path loss at the reference distance of 1 m is set as 30 dB. Other system parameters are

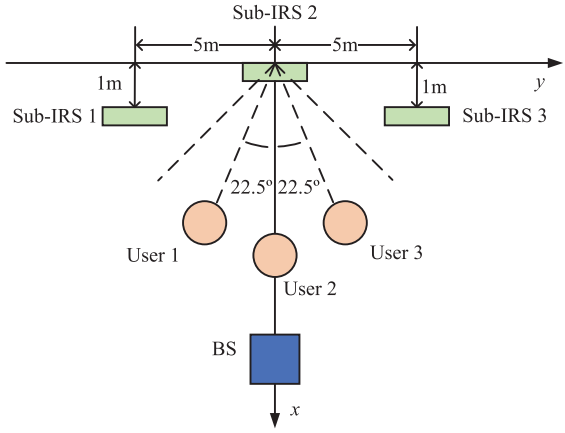

Fig. 5. Simulation setup (top view).

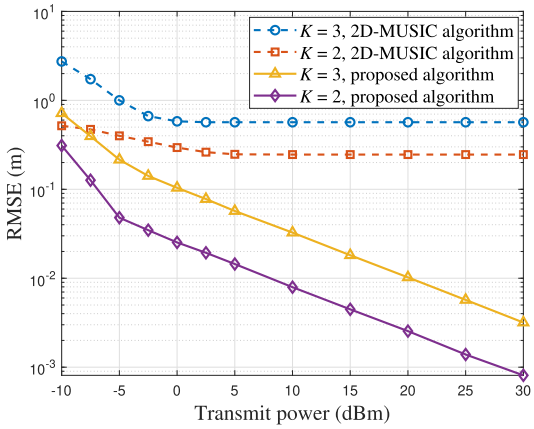

Fig. 6. RMSE of the estimated users' locations versus transmit power.

set as follows: $K = 3$, $N = 8$, $M_1 = 32 \times 32$, $M_2 = M_3 = M_{\mathrm{semi}} = 12 \times 12$, $T = 1200$, $T_1 = 120$, $\tau_1 = 20$, $\epsilon_{\mathrm{I2B}} = 2.3$, $\epsilon_{\mathrm{U2I}} = 2.2$, $\epsilon_{\mathrm{I2I}} = 2.1$, $b = 3$, $b_\Delta = 4$, $S_{\mathrm{ISAC}} = 1500$, $S_{\mathrm{ISAC}}^{\mathrm{elite}} = 300$, $S_{\mathrm{PC}} = 2000$, $S_{\mathrm{PC}}^{\mathrm{elite}} = 400$, $\kappa = 10^{-4}$, $C = 4$, $\rho = 20$ dBm and $\sigma_0^2 = -80$ dBm (if not specified otherwise).

A. Performance of Multi-User Location Sensing

Without loss of generality, we focus on the localization during the first time block of the ISAC period. We adopt the root mean square error (RMSE) to measure the performance of localization,

$$\varepsilon = \mathbb{E}\left\{\sqrt{\frac{1}{K}\sum\nolimits_{k=1}^{K} \|\hat{\mathbf{q}}_{\mathrm{U},k} - \mathbf{q}_{\mathrm{U},k}\|^2}\right\}. \tag{79}$$

Fig. 6 shows the RMSE of the estimated users' locations versus the transmit power with different numbers of users. For comparison, the 2D-MUSIC algorithm is presented, where the AoA pairs are determined by exhaustive search in a 2^{16}-element set $\mathcal{G} = \{(u - \pi, v - \pi) | u, v \in \mathcal{F}_8\}$. It is obvious that the proposed algorithm performs much better than the 2D-MUSIC algorithm. On the one hand, as the transmit power increases, the localization accuracy of the proposed algorithm improves significantly, while that of the 2D-MUSIC algorithm improves at first and soon

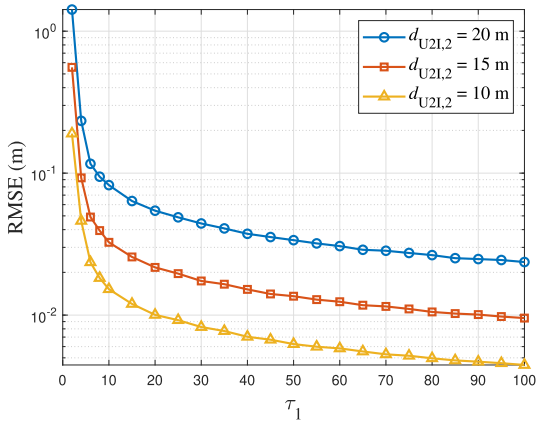

Fig. 7. RMSE of the estimated users' locations versus sensing time.

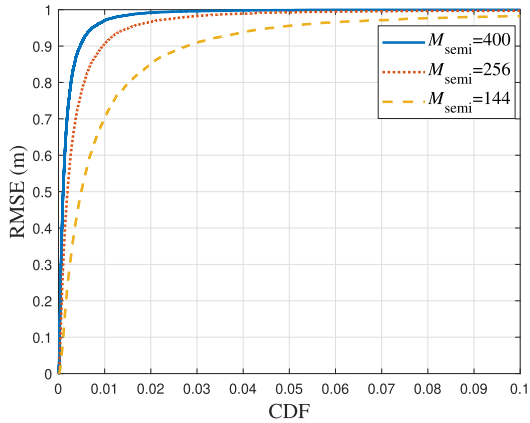

Fig. 8. CDF curves of the RMSE.

achieves the error floor due to the limitation of the exhaustive search's precision. On the other hand, with the AoA quantization accuracy of G bits, the 2D-MUSIC algorithm requires 2^{2G} AoA searches, while the proposed algorithm only requires $(K+1)^2$ AoA searches, which significantly reduces the complexity of localization. In addition, increasing the number of users leads to a lower localization accuracy. For instance, the localization accuracy is reduced by six times as the number of users increases from 2 to 3. This is because, with a given number of semi-passive elements, the path discrimination capability of the semi-passive IRS is fixed. With more users, the semi-passive sub-IRS has to distinguish more user-IRS paths, which would reduce the accuracy of the estimated effective AoAs corresponding to each user-IRS path.

Fig. 7 presents the RMSE of the estimated users' locations versus the sensing time (i.e., τ_1) with different user-IRS distances. For all three configurations of user-IRS distances, the RMSE of the estimated users' locations decreases as the sensing time becomes larger. This is because collecting more data can help suppress the adverse effect of noise, thereby improving the localization accuracy. Besides, the localization accuracy degrades with the increase of the user-IRS distance. This performance degradation can be compensated by increasing sensing time. For instance, when $d_{\mathrm{U2I},2}$ increases from 10 m to 15 m, the RMSE remains unchanged at 10^{-2} by increasing τ_1 from about 20 to 90.

Finally, in Fig. 8, we illustrate the cumulative distribution function of the RMSE by considering that all users are randomly distributed in a square centered at (4 m, 0 m, 0 m) with the side length of 10 m. For all three configurations of numbers of semi-passive elements, the proposed multi-user location sensing algorithm achieves a high positioning accuracy of at least 3 cm with the probability of 90%. Moreover, by increasing the number of semi-passive elements to 400, a millimeter-level localization accuracy is achieved with the probability of 90%, due to a high spatial resolution.

B. Performance of the Proposed Sensing-Based Beamforming Algorithms

In this subsection, numerical results are presented to illustrate the effectiveness and convergence of the proposed beamforming algorithms in the ISAC and PC periods, respectively. For comparison, the alternating optimization (AO) algorithm [12] with continuous phase shifts and perfect CSI, the low complexity local search (LS) algorithm [14] with perfect CSI, as well as the random phase shift algorithm are presented as three benchmarks for both ISAC and PC periods. In addition, the ZF-based beamforming algorithm is presented as a benchmark for the ISAC period, to demonstrate the advantage of the proposed MRC-based beamforming algorithm in the ISAC period. The sum rates in the ISAC and PC periods are respectively defined as

$$\bar{R}_{\mathrm{ISAC}} = \mathbb{E}\left\{R(t)\right\}, t \in \{1, 2, \ldots, T_1\}, \tag{80}$$

$$\bar{R}_{\mathrm{PC}} = \mathbb{E}\left\{R(t)\right\}, t \in \{T_1+1, T_1+2, \ldots, T_1+T_2\}. \tag{81}$$

Fig. 9(a) and (b) compare the sum rates of different beamforming algorithms versus the number of IRS elements operating in the reflecting mode.It is obvious that the proposed algorithm with discrete phase shifts and sensed location information is superior to the LS algorithm and the random phase shift algorithm, and even achieves comparable performance to the AO algorithm with continuous phase shifts and perfect CSI. Moreover, with the increase of the number of IRS elements, all beamforming algorithms except for the random phase shift algorithm achieve significant performance gains, especially in the case of a small number of IRS elements. For the proposed algorithm and the AO algorithm, the sum rate achieved in the PC period is much larger than that achieved in the ISAC period even with the same number of IRS elements operating in the reflecting mode. This is because there are more distributed sub-IRSs assisting uplink data transmission in the PC period, thereby providing a larger spatial multiplexing gain. In contrast, the LS algorithm and the random phase shift algorithm perform worse in the PC period, thus are not suitable for multiple IRS scenarios. In addition, we can observe from Fig. 9(a) that the proposed MRC-based beamforming algorithm for the ISAC period performs slightly better than the ZF-based beamforming algorithm. This is because the channel between the BS and IRS is rank-one with only one passive sub-IRS used for communication during the ISAC period. As such, the multi-user interference can not be effectively eliminated by using the ZF-based beamforming

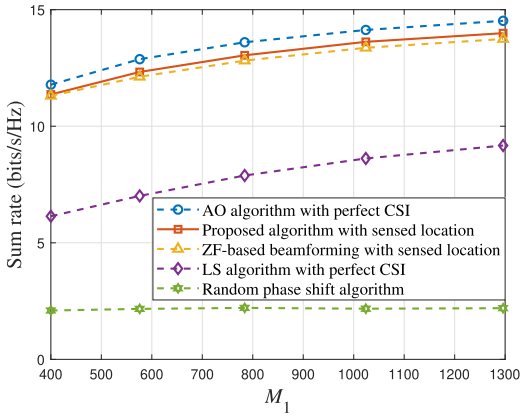

(a) ISAC period.

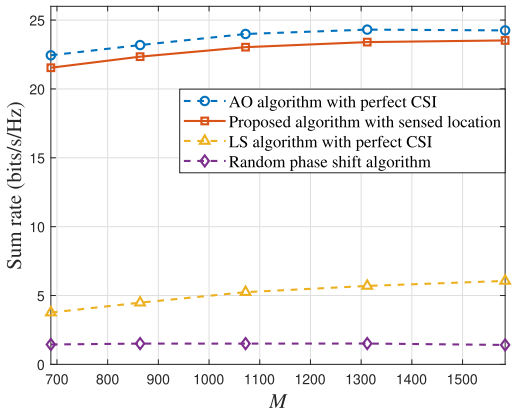

(b) PC period.

Fig. 9. Sum rate versus the number of IRS elements operating in the reflecting mode.

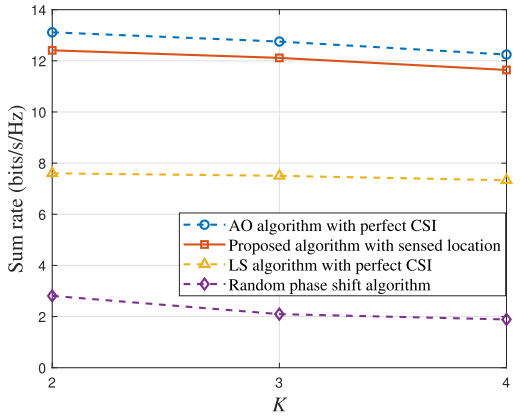

(a) ISAC period.

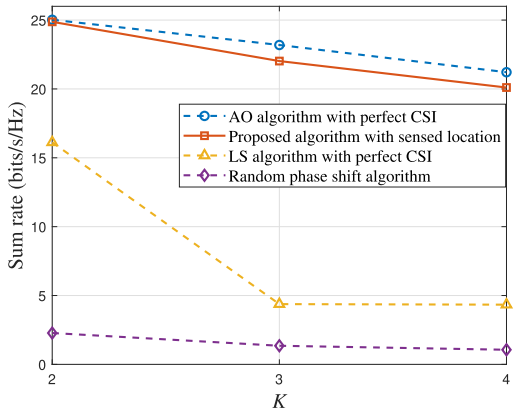

(b) PC period.

Fig. 10. Sum rate versus the number of users K.

algorithm, leading to worse communication performance than the proposed MRC-based beamforming algorithm.

Fig. 10(a) and (b) compare the sum rates of different beamforming algorithms versus the user number K, where we set the total transmit power of K users to be 20 dBm (i.e., $K\rho =$ 20 dBm) and $M_{\text{semi}} = 16 \times 16$. In both ISAC and PC periods, the performance of all four beamforming algorithms degrades with the increase of the user number, especially for the LS algorithm. For the AO algorithm, the LS algorithm as well as the random phase shift algorithm, this performance degradation is due to more inter-user interference, while for the proposed beamforming algorithm, this performance degradation is due to both more inter-user interference and less accurate sensed users' locations.

Fig. 11(a) and (b) illustrate the convergence of the proposed beamforming algorithms with different numbers of IRS elements and bit-quantization numbers. We can observe that the proposed two beamforming algorithms converge for any number of IRS elements and quantization bits. Adding more IRS elements decreases the convergence speed, due to the increased number of optimization variables. Also, as the bit-quantization number increases, the convergence speed becomes slower, due to the enlarged searching region of IRS phase shifts.

C. Performance of the IRS-Enabled Multi-User ISAC System

Fig. 12 illustrates the sum rate in the ISAC period versus τ_1/T_1 with different values of ρ, where we set $T_1 : T = \frac{1}{10}$ and $T = 2000$. The optimal ratio of time allocation indicates that, it is desirable to allocate a small portion of time slots to the first time block and more time slots to the second time block. This is because the CSI is unavailable in the first time block, while location information is available in the second time block, which can be used for more effective beamforming design. Moreover, the optimal ratio τ_1/T_1 decreases with the transmit power. With a larger transmit power, the positioning accuracy is sufficiently high and thus it is unnecessary to allocate too much time to the first time block. However, with too little time allocated to the first time block, the communication performance would degrade significantly, due to the fact that low-accuracy localization in the first time block would affect the effectiveness of beamforming design in the second time block.

Fig. 13 presents the sum rate in the whole transmission period versus the ratio T_1/T with different ρ, where $\tau_1/T_1 = \frac{1}{10}$, $T =$ 1000, and the sum rate is defined as

$$\bar{R} = \mathbb{E}\left\{R(t)\right\}, t \in \left\{1, 2, \ldots, T_1 + T_2\right\}. \tag{82}$$

The optimal ratio decreases as the transmit power becomes larger. For instance, with a lower power of -5 dBm, the optimal

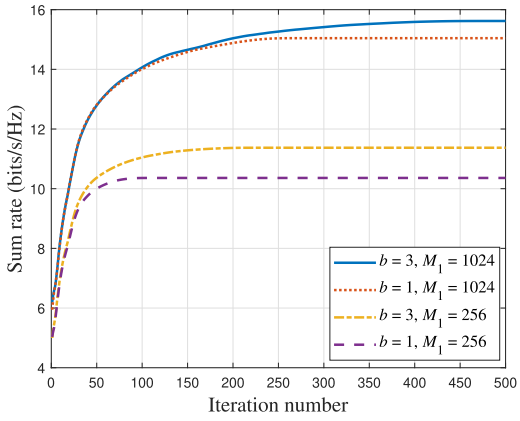

(a) ISAC period.

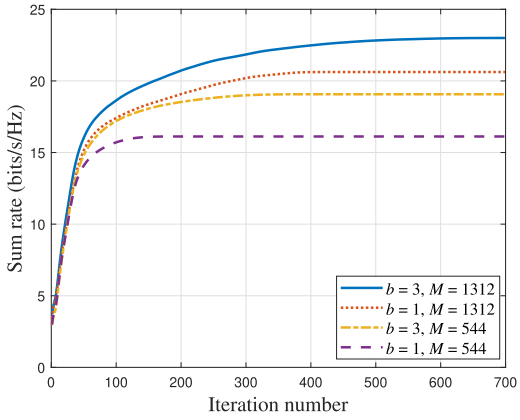

(b) PC period.

Fig. 11. Convergence of the proposed beamforming algorithms.

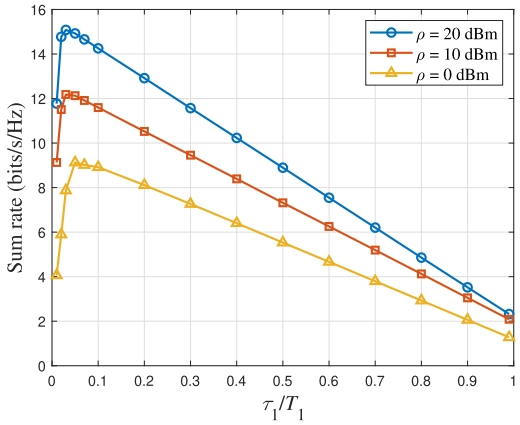

Fig. 12. Sum rate of the ISAC period versus τ_1/T_1.

T_1/T is about 1, which indicates that simultaneous location sensing and communication should be conducted during the whole transmission period. As the transmit power increases to 5 dBm, the optimal T_1/T drops to 0.2. With the highest transmit power of 25 dBm, the optimal ratio approaches 0. This is because with high transmit power, an enough high sensing accuracy can be achieved in a short time.

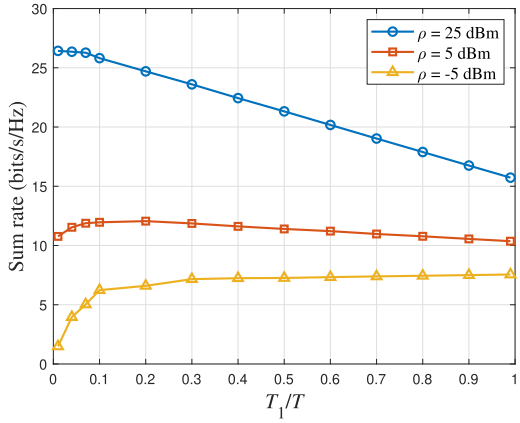

Fig. 13. Sum rate of the transmission period versus T_1/T.

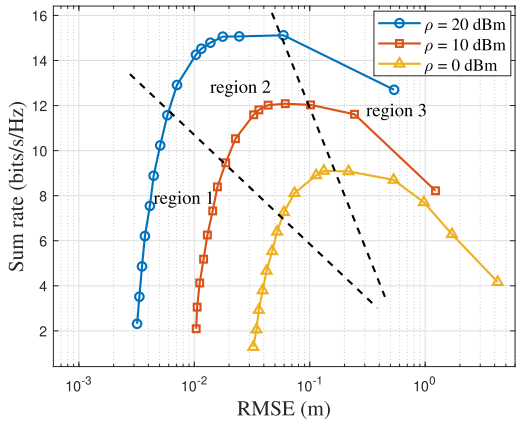

Fig. 14. Trade-off between communication performance and localization performance of the ISAC period.

Finally, Fig. 14 shows the trade-off between the communication performance and localization performance of the ISAC period with different values of ρ, where we set $T_1 : T = \frac{1}{10}$ and $T = 2000$. We can observe that for all three configurations of transmit power, the communication-localization curve includes three regions. Specifically, in region 1, the localization performance is nearly saturated. Despite sacrificing the communication performance a lot, a little localization performance gain can be obtained. For example, when $\rho = 10$ dBm, despite sacrificing the sum rate from 9.5 bits/s/Hz to 2 bits/s/Hz, the localization accuracy can only be improved by less than twice. In region 2, the communication performance and the localization performance are properly balanced, and sacrificing the performance of one can effectively enhance that of another. For example, when $\rho = 20$ dBm, sacrificing the sum rate from 15.1 bits/s/Hz to 11.6 bits/s/Hz can achieve 10 times higher localization accuracy. In region 3, the location sensing accuracy is too low to promise the effectiveness of the sensing-based beamforming design, thus leading to an unsatisfying communication performance. Hence, in this scenario, it is suggested to allocate more resources to localization for promising good performance of both communication and localization.

VII. Conclusion

In this paper, we proposed an IRS-enabled multi-user ISAC framework, and designed its working process, including the transmission protocol, multi-user location sensing as well as joint active and passive beamforming. Specifically, we first designed an ISAC transmission protocol, where the considered transmission period consists of the ISAC period for multi-user simultaneous communication and localization and the PC period for uplink data transmission. Then, we proposed a multi-user location sensing algorithm, by using uplink communication signals sent by multiple users to the BS. Based on the sensed users' locations, two novel beamforming algorithms were proposed to maximize the sum rate for the ISAC period and the PC period, respectively. Numerical results demonstrated that the proposed multi-user location sensing algorithm can provide millimeter-level accuracy with a high probability of 90%. By increasing the number of semi-passive elements or sensing time, the positioning accuracy can be further improved. Moreover, despite imperfect CSI and discrete phase shifts, the proposed two sensing-based beamforming algorithms achieve comparable performance to the benchmark with perfect CSI and continuous phase shifts, demonstrating the effectiveness of beamforming designs using sensed location information. In addition, we have investigated the overall communication performance of the IRS-enabled ISAC system, and numerical results showed that the optimal time ratio of the ISAC period to the PC period decreases with the increase of transmit power, indicating that less time should be allocated to the ISAC period when transmit power is high.

References

[1] Y. Liu et al., "Reconfigurable intelligent surfaces: Principles and opportunities," *IEEE Commun. Surv. Tut.*, vol. 23, no. 3, pp. 1546–1577, Jul.–Sep. 2021.

[2] Q. Wu and R. Zhang, "Intelligent reflecting surface enhanced wireless network via joint active and passive beamforming," *IEEE Trans. Wireless Commun.*, vol. 18, no. 11, pp. 5394–5409, Nov. 2019.

[3] S. Gong et al., "Toward smart wireless communications via intelligent reflecting surfaces: A contemporary survey," *IEEE Commun. Surv. Tut.*, vol. 22, no. 4, pp. 2283–2314, Oct.–Dec. 2020.

[4] Q. Wu and R. Zhang, "Towards smart and reconfigurable environment: Intelligent reflecting surface aided wireless network," *IEEE Commun. Mag.*, vol. 58, no. 1, pp. 106–112, Jan. 2020.

[5] C. Pan et al., "Reconfigurable intelligent surfaces for 6G systems: Principles, applications, and research directions," *IEEE Commun. Mag.*, vol. 59, no. 6, pp. 14–20, Jun. 2021.

[6] C. You, B. Zheng, and R. Zhang, "Channel estimation and passive beamforming for intelligent reflecting surface: Discrete phase shift and progressive refinement," *IEEE J. Select. Areas Commun.*, vol. 38, no. 11, pp. 2604–2620, Nov. 2020.

[7] X. Yu, D. Xu, and R. Schober, "MISO wireless communication systems via intelligent reflecting surfaces," in *Proc. IEEE/CIC Int. Conf. Commun. China*, Changchun, China, 2019, pp. 735–740.

[8] S. Zhou, W. Xu, K. Wang, M. Di Renzo, and M.-S. Alouini, "Spectral and energy efficiency of IRS-assisted MISO communication with hardware impairments," *IEEE Wireless Commun. Lett.*, vol. 9, no. 9, pp. 1366–1369, Sep. 2020.

[9] L. You, J. Xiong, D. W. K. Ng, C. Yuen, W. Wang, and X. Gao, "Energy efficiency and spectral efficiency tradeoff in RIS-aided multiuser MIMO uplink transmission," *IEEE Trans. Signal Process.*, vol. 69, pp. 1407–1421, 2021.

[10] C. Pan et al., "Intelligent reflecting surface aided MIMO broadcasting for simultaneous wireless information and power transfer," *IEEE J. Sel. Areas Commun.*, vol. 38, no. 8, pp. 1719–1734, Aug. 2020.

[11] G. Zhou, C. Pan, H. Ren, K. Wang, and A. Nallanathan, "Intelligent reflecting surface aided multigroup multicast MISO communication systems," *IEEE Trans. Signal Process.*, vol. 68, pp. 3236–3251, 2020.

[12] H. Guo, Y.-C. Liang, J. Chen, and E. G. Larsson, "Weighted sum-rate maximization for reconfigurable intelligent surface aided wireless networks," *IEEE Trans. Wireless Commun.*, vol. 19, no. 5, pp. 3064–3076, May 2020.

[13] S. Wang, Q. Li, S. X. Wu, and J. Lin, "Sum rate maximization for multiuser MISO downlink with intelligent reflecting surface," *arXiv:1912.09315*.

[14] W. Chen, X. Ma, Z. Li, and N. Kuang, "Sum-rate maximization for intelligent reflecting surface based terahertz communication systems," in *Proc. IEEE/CIC Int. Conf. Commun. Workshops China*, Changchun, China, 2019, pp. 153–157.

[15] C. Huang, A. Zappone, G. C. Alexandropoulos, M. Debbah, and C. Yuen, "Reconfigurable intelligent surfaces for energy efficiency in wireless communication," *IEEE Trans. Wireless Commun.*, vol. 18, no. 8, pp. 4157–4170, Aug. 2019.

[16] M. Zeng, E. Bedeer, O. A. Dobre, P. Fortier, Q.-V. Pham, and W. Hao, "Energy-efficient resource allocation for IRS-assisted multi-antenna uplink systems," *IEEE Wireless Commun. Lett.*, vol. 10, no. 6, pp. 1261–1265, Jun. 2021.

[17] M. Forouzanmehr, S. Akhlaghi, A. Khalili, and Q. Wu, "Energy efficiency maximization for IRS-assisted uplink systems: Joint resource allocation and beamforming design," *IEEE Commun. Lett.*, vol. 25, no. 12, pp. 3932–3936, Dec. 2021.

[18] F. Fang, Y. Xu, Q.-V. Pham, and Z. Ding, "Energy-efficient design of IRS-NOMA networks," *IEEE Trans. Veh. Technol.*, vol. 69, no. 11, pp. 14088–14092, Nov. 2020.

[19] S. Hu, F. Rusek, and O. Edfors, "Beyond massive MIMO: The potential of positioning with large intelligent surfaces," *IEEE Trans. Signal Process.*, vol. 66, no. 7, pp. 1761–1774, Apr. 2018.

[20] J. He, H. Wymeersch, L. Kong, O. Silvén, and M. Juntti, "Large intelligent surface for positioning in millimeter wave MIMO systems," in *Proc. IEEE 91st Veh. Technol. Conf. (VTC2020-Spring)*, Antwerp, Belgium, 2020, pp. 1–5.

[21] J. He, H. Wymeersch, T. Sanguanpuak, O. Silvén, and M. Juntti, "Adaptive beamforming design for mmWave RIS-aided joint localization and communication," in *Proc. IEEE Wireless Commun. Netw. Conf. Workshops*, Seoul, Korea, 2020, pp. 1–6.

[22] A. Elzanaty, A. Guerra, F. Guidi, and M.-S. Alouini, "Reconfigurable intelligent surfaces for localization: Position and orientation error bounds," *IEEE Trans. Signal Process.*, vol. 69, pp. 5386–5402, 2021.

[23] H. Zhang, H. Zhang, B. Di, K. Bian, Z. Han, and L. Song, "Metalocalization: Reconfigurable intelligent surface aided multi-user wireless indoor localization," *IEEE Trans. Wireless Commun.*, vol. 20, no. 12, pp. 7743–7757, Dec. 2021.

[24] W. Wang and W. Zhang, "Joint beam training and positioning for intelligent reflecting surfaces assisted millimeter wave communications," *IEEE Trans. Wireless Commun.*, vol. 20, no. 10, pp. 6282–6297, Oct. 2021.

[25] H. Zhang, H. Zhang, B. Di, K. Bian, Z. Han, and L. Song, "Towards ubiquitous positioning by leveraging reconfigurable intelligent surface," *IEEE Commun. Lett.*, vol. 25, no. 1, pp. 284–288, Jan. 2021.

[26] R. Wang, Z. Xing, and E. Liu, "Joint location and communication study for intelligent reflecting surface aided wireless communication system," *arXiv:2103.01063*.

[27] A. Taha, M. Alrabeiah, and A. Alkhateeb, "Enabling large intelligent surfaces with compressive sensing and deep learning," *IEEE Access*, vol. 9, pp. 44304–44321, 2021.

[28] S. Liu, Z. Gao, J. Zhang, M. D. Renzo, and M.-S. Alouini, "Deep denoising neural network assisted compressive channel estimation for mmwave intelligent reflecting surfaces," *IEEE Trans. Veh. Technol.*, vol. 69, no. 8, pp. 9223–9228, Aug. 2020.

[29] C. Qian et al., "Dynamic recognition and mirage using neuro-metamaterials," *Nature Commun.*, vol. 13, no. 1, pp. 1–8, May 2022.

[30] Z. Fan et al., "Homeostatic neuro-metasurfaces for dynamic wireless channel management," *Sci. Adv.*, vol. 8, no. 27, Jul. 2022, Art. no. eabn7905.

[31] R. Liu, M. Li, and A. L. Swindlehurst, "Joint beamforming and reflection design for ris-assisted isac systems," *arXiv:2203.00265*.

[32] Z.-M. Jiang et al., "Intelligent reflecting surface aided dual-function radar and communication system," *IEEE Syst. J.*, vol. 16, no. 1, pp. 475–486, Mar. 2022.

[33] J. Yuan, Y.-C. Liang, J. Joung, G. Feng, and E. G. Larsson, "Intelligent reflecting surface-assisted cognitive radio system," *IEEE Trans. Commun.*, vol. 69, no. 1, pp. 675–687, Jan. 2021.
[34] H. L. Van Trees, *Optimum Array Processing: Part IV of Detection, Estimation, and Modulation Theory*. Hoboken, NJ, USA: Wiley, 2004.
[35] S. Jung, C. oh Lee, and D. Han, "Wi-Fi fingerprint-based approaches following log-distance path loss model for indoor positioning," in *Proc. IEEE MTT-S Int. Microw. Workshop Ser. Intell. Radio Future Pers.* Terminals, Daejeon, 2011, pp. 1–2.
[36] X. Chen and Z. Zhang, "Exploiting channel angular domain information for precoder design in distributed antenna systems," *IEEE Trans. Signal Process.*, vol. 58, no. 11, pp. 5791–5801, Nov. 2010.
[37] H. Mühlenbein, "The equation for response to selection and its use for prediction," *Evol. Comput.*, vol. 5, no. 3, pp. 303–346, Sep. 1997.

Zhouyuan Yu received the B.E. degree in communication engineering from the Nanjing University of Posts and Telecommunications, Nanjing, China, in 2021. He is currently working toward the Ph.D. degree with the State Key Laboratory of Networking and Switching Technology, Beijing University of Posts and Telecommunications, Beijing, China. His research interests include reconfigurable intelligent surface, integrated sensing and communication, and wireless sensing.

Xiaoling Hu (Member, IEEE) received the B.E. degree in electronics and information engineering from the Dalian University of Technology, Dalian, China, in 2016, and the Ph.D. degree in information and communication engineering from Zhejiang University, Hangzhou, China, in 2021. She is currently an Associate Professor with the Beijing University of Posts and Telecommunications, Beijing, China. Her research interests include reconfigurable intelligent surface, integrated sensing and communication, wireless sensing, massive MIMO, and mmWave. She and her coauthors was the recipient of Best Paper Award at the IEEE GLOBECOM 2020, IEEE ICC 2019, and IEEE ICC 2022.

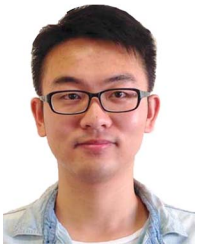

Chenxi Liu (Senior Member, IEEE) received the B.E. degree from Central South University, Changsha, China, in 2010, and Ph.D. degree from the University of New South Wales, Sydney, NSW, Australia, in 2016. From 2017 to 2019, he was a Postdoctoral Research Fellow with the Singapore University of Technology and Design, Singapore. Since 2019, he has been with the Beijing University of Posts and Telecommunications, Beijing, China, where he is currently an Associate Professor. His research interests include wireless security, unmanned aerial vehicle-enabled wireless networks, and network intelligence. He was the recipient of the Best Paper Award from the IEEE ICC 2022. He is currently the Editor of the IEEE WIRELESS COMMUNICATIONS LETTERS.

Mugen Peng (Fellow, IEEE) received the Ph.D. degree in communication and information systems from the Beijing University of Posts and Telecommunications (BUPT), Beijing, China, in 2005. Afterward, he joined BUPT, where he has been the Dean of the School of Information and Communication Engineering since June 2020, and Deputy Director of State Key Laboratory of Net-working and Switching Technology since October 2018. In 2014 he was also an academic Visiting Fellow with Princeton University, Princeton, NJ, USA. He has authored and coauthored more than 150 refereed IEEE journal papers and more than 250 conference proceeding papers. His research interests include wireless communication theory, radio signal processing, cooperative communication, self-organization networking, cloud communication, and Internet of Things. Prof. Peng was the recipient of the 2018 Heinrich Hertz Prize Paper Award, 2014 IEEE ComSoc AP Outstanding Young Researcher Award, and Best Paper Award in the IEEE ICC 2022, JCN 2016, IEEE WCNC 2015, IEEE GameNets 2014, IEEE CIT 2014, ICCTA 2011, IC-BNMT 2010, and IET CCWMC 2009. He is on the Editorial/Associate Editorial Board of the IEEE COMMUNICATIONS MAGAZINE, the IEEE INTERNET OF THINGS JOURNAL, the IEEE TRANSACTIONS ON VEHICULAR TECHNOLOGY, and the IEEE TRANSACTIONS ON NETWORK SCIENCE AND ENGINEERING.

Caijun Zhong (Senior Member, IEEE) received the B.S. degree in information engineering from the Xi'an Jiaotong University, Xi'an, China, in 2004, and the M.S. degree in information security and the Ph.D. degree in telecommunications from University College London, London, U.K., in 2006 and 2010, respectively. From September 2009 to 2011, he was a Research Fellow with the Institute for Electronics, Communications and Information Technologies, Queens University Belfast, Belfast, U.K. Since September 2011, he has been with Zhejiang University, Hangzhou, China, where he is currently a Professor. His research interests include reconfigurable intelligent surfaces assisted communications and artificial intelligence based wireless communications. He is the Editor of *Science China: Information Science* and *China Communications*. He was the Editor of the IEEE TRANSACTIONS ON WIRELESS COMMUNICATIONS and IEEE COMMUNICATIONS LETTERS. He was the recipient of the 2013 IEEE ComSoc Asia-Pacific Outstanding Young Researcher Award. He and his coauthors was the recipient of the Best Paper Award at the IEEE GLOBECOM 2020 and IEEE ICC 2019.